THE EUROPEAN
PHYSICAL JOURNAL C

Regular Article - Theoretical Physics

Acoustic regular black hole in fluid and its similarity and diversity to a conformally related black hole

Chen Lan[a] , Yan-Gang Miao[b], Yi-Xiong Zang[c]

School of Physics, Nankai University, Tianjin 300071, China

Abstract We address an interesting question in the present paper that whether the acoustic gravity can be applied as a tool to the study of regular black holes. For this purpose, we construct a general acoustic regular black hole in the spherically symmetric fluid, where its regularity is verified from the perspective of finiteness of curvature invariants and completeness of geodesics. In particular, we find that the acoustic interval not only looks like a line element of a conformally related black hole in which the fluid density can be regarded as a conformal factor, but also gives rise to a non-vanishing partition function which coincides with that of a conformally related black hole. As an application, we provide a specific acoustic regular black hole model, investigate its energy conditions and compute its quasinormal modes. We note that the strong energy condition of our model is violated completely outside the horizon of the model but remains valid in some regions inside the horizon, which may give a new insight into the relation between the regularity and strong energy condition. Moreover, we analyze the oscillating and damping features of our model when it is perturbed.

1 Introduction

Since the Hawking radiation from black holes (BHs) was discovered [1], it has become one of the central subjects to study the quantum behaviors of BHs. However, this thermal radiation is too small to be directly detected by any conceivable experiments. When the Schwarzschild BH with one solar mass is taken as an example, its radiation temperature is approximately 6×10^{-8} K, while the cosmic background is of 3 K microwave radiation. Therefore, the former is completely covered up by the latter. In other words, even if the thermal radiation is emitted, it will be

drowned out by the background noise. This situation motivates the researches to shift from astrophysical phenomena to their analogues in laboratories on Earth, which was pioneered by Unruh [2] who proposed an acoustic analogy.

An acoustic black hole (ABH), being one of the realizations of analogue BHs, can be formed in laboratories on Earth when the velocity of moving fluid exceeds the local velocity of sound, where the horizon is located [3] at the junction of the supersonic and subsonic regions. Several attempts have been done in recent decades, including surface waves in Bose-Einstein condensates [4], water flows [5], optical systems [6], quantum many-body systems [7], and so on. For the early progress in analogue BHs, see, for instance, the review article [8] and the references therein. Recently, there have been many theoretical and experimental advances in various aspects of analogue gravity, such as in the Hawking radiation [9–13], the superradiation [14–16], the quasinormal modes (QNMs) [17], and the Lyapunov exponent [18], etc. Moreover, ABHs have been generalized [19] to curved spacetimes. In particular, the experimental advances reflect the applicability of analogue gravity.

Although the analogue gravity has been developed and regarded as a tool of gaining insight into general relativity, the first simulation of Schwarzschild and Reissner–Nordström BHs was not realized until 2021 [20]. Prior to this work, some analogue BH models, such as the draining bathtub model [3,21], may contain the necessary features that give rise to the astronomical phenomena, but can hardly have the direct counterparts in the universe. And the differences between astronomical black holes and their acoustic counterparts may appear distinctly in the desired phenomena in the earth laboratory. For instance, in the acoustic simulation of the Painlevé–Gullstrand spacetime [8], the astronomical metric differs from the acoustic one by a conformal factor. Thus, the study of the quasi-normal modes from the acoustic counterpart may not provide the full information of spectra

a e-mail: lanchen@nankai.edu.cn

b e-mail: miaoyg@nankai.edu.cn (corresponding author)

c e-mail: zangyx@mail.nankai.edu.cn

Springer

for the Painlevé–Gullstrand geometry, because the conformal factor affects the quasi-normal modes except in the eikonal limit [22].

Moreover, it is widely known that singular black holes (SBHs) suffer [23] from the UV incompleteness at both classical and quantum levels because of the spacetime singularity. Many phenomenological models have been proposed for avoiding the singularity at the center of BHs, see, for instance, the review [24]. These nonsingular solutions of general relativity are called regular black holes (RBHs), being of finite curvature invariants on the entire manifold of spacetime. In fact, Bardeen proposed [25] the first RBH which was recognized [26] later on as a product created by nonlinear electrodynamics (NED). This model is currently dubbed as Bardeen black hole (BBH). The further developments of the BBH have been presented, see, e.g., Refs. [27–29]. Besides the BBH, the other RBHs have also been proposed [30–32].

Our aim in the current work is to construct RBHs in acoustic gravity named as acoustic RBHs (ARBHs) and to investigate their energy conditions and dynamic properties, such as QNMs [33]. Here we note that the energy conditions refer to the constrains on the matters generating the RHBs in the Universe, not on the fluid for simulation in a laboratory. Since we dedicate to study the RBHs with the aid of analogue gravity, we investigate whether the RBHs we construct in fluid are reasonable or not, that is, if their counterparts in the Universe have the possibility of existence. As a by-product, we find that ARBHs have different characteristics from those of RHBs generated by NED, in particular, they should be classified into conformal gravity [34–36]. The seeming reason is that the acoustic interval looks like a line element of a conformally related black hole, where the fluid density can be regarded as a conformal factor, but the virtual reason is that the acoustic interval leads to a non-vanishing partition function if it is interpreted in the context of conformally invariant theory.

In general relativity, the energy conditions give [37,38] constraints upon the energy–momentum tensor of matter fields, such as positivity of energy density and validity of causality. For instance, one can determine whether the matter field of RBHs created by NED is physically reasonable in terms of the dominant energy condition and whether the superradiance occurs by checking the weak energy condition which is also associated with the second law of BH mechanics [39]. In the context of ARBHs, we define the analogue energy–momentum $T_{\mu\nu}$ and thus explore the corresponding energy conditions by supposing the linear relation between the analogue Einstein tensor and energy–momentum tensor. We find that the energy conditions of ARBHs have novel properties when ARBHs are dealt with in the framework of conformal gravity.

As QNMs play an important role in the stability analysis of analogue BHs, see, for instance, an example of optical BHs [40], we focus on the QNMs of ARBHs by studying the propagation of scalar fields in the effective curved spacetime manifested as the acoustic disturbance. As shown in Ref. [2], the equation of motion for the acoustic disturbance is identical to the d'Alembertian equation of a massless scalar field propagating in a curved spacetime. We can thus compute the QNM frequencies of ARBHs by using the WKB method [41–45] as usual.

This paper is organized as follows. We propose a general method to construct ARBHs in Sect. 2, where the regularity is verified in the perspective of finiteness of curvature invariants and completeness of geodesics. We then give one specific ARBH model in Sect. 3. In Sect. 4, based on the complete form of Euler's equation we analyze the importance of an external-force term in the realization of acoustic analogy. The energy conditions of the model are discussed and compared with those of the conformally related Schwarzschild black holes (CRSBHs) [35] in Sect. 5. In Sect. 6, we analyze the effective potential and calculate the QNMs for the ARBH model. Finally, we give our summary in Sect. 7. The Appendices A and B include the detailed analyses of energy conditions of CRSBHs and the repulsive interaction of the specific ARBH model outside the model's event horizon. Throughout this paper, we adopt the units with the speed of sound $c = 1$ and the sign convention $(-, +, +, +)$.

2 Acoustic regular black hole in fluid

In this section, we construct a general ARBH in the spherically symmetric fluid. The fluid is assumed to be locally irrotational, barotropic, inviscid, and compressible. The acoustic interval then takes the form [8],

$$ds^2 = \frac{\rho}{c} \left[-c^2 dt^2 + (d\boldsymbol{x} - \boldsymbol{v}dt)^2 \right], \tag{1}$$

which can be obtained by combining the equation of continuity,

$$\partial_t \rho + \nabla \cdot (\rho \boldsymbol{v}) = 0, \tag{2}$$

and Euler's equation,

$$\rho \left[\partial_t \boldsymbol{v} + (\boldsymbol{v} \cdot \nabla)\boldsymbol{v} \right] = -\nabla p - \rho \nabla \psi, \tag{3}$$

where ρ, $\boldsymbol{v}$, and p are density, velocity, and pressure of the fluid, respectively, and $c \equiv \sqrt{|\partial p/\partial \rho|}$ is local speed of sound. In the following discussions c is normalized to unity,[1] and the density ρ and velocity $\boldsymbol{v}$ are supposed to be functions of radial coordinate r only. In addition, the last term of Eq. (3) represents [3] an external driving force and ψ is the corresponding potential. This term does not affect [3] the wave equation of sound and the acoustic metric, but it is

---

[1] In general, the local speed of sound depends mainly on the temperature of fluid. Here the temperature of fluid is constant, so it is usual to set $c = 1$.

indispensable in the acoustic analogue of an astronomical black hole because ψ provides an external field for realizing the specific fluid, which will be explained in detail in Sect. 4.

If we consider the spherically symmetric fluid with only non-vanishing radial velocity, $v_r \neq 0$, and perform the following transformation,

$$dt \to d\tilde{t} - \frac{v_r}{1 - v_r^2} dr, \tag{4}$$

we rewrite Eq. (1) as follows,

$$ds^2 = \rho \left(-f d\tilde{t}^2 + f^{-1} dr^2 + r^2 d\theta^2 + r^2 \sin^2 \theta d\phi^2 \right), \tag{5}$$

or write the metric explicitly,

$$g_{\mu\nu} = \rho \tilde{g}_{\mu\nu}, \qquad \tilde{g}_{\mu\nu} \equiv \operatorname{diag} \left\{ -f, f^{-1}, r^2, r^2 \sin^2 \theta \right\},$$
$$f \equiv 1 - v_r^2. \tag{6}$$

The density ρ plays the role of a conformal factor if $\tilde{g}_{\mu\nu}$

- (i) ρ is divergent, while v_r is finite;[3]
- (ii) ρ is finite, while v_r is divergent;
- (iii) Both ρ and v_r are divergent.

Such a classification will help us construct ARBHs.

In order to check whether $g_{\mu\nu}$, see Eq. (6), together with Eq. (7) describes an ARBH or not, we have to investigate the finiteness of curvature invariants and completeness of geodesics at the center of this ARBH. Next, we discuss the two issues in two separate subsections.

2.1 Finiteness of curvature invariants

Using Eq. (6) and the definitions of the three curvature invariants, the Ricci scalar $R \equiv g^{\mu\nu} R_{\mu\nu}$, the contraction of two Ricci tensors $R_2 \equiv R_{\mu\nu} R^{\mu\nu}$, and the Kretschmann scalar $K \equiv R_{\mu\nu\rho\sigma} R^{\mu\nu\rho\sigma}$, we obtain

$$R = \frac{3 f \rho'^2}{2\rho^3} - \frac{3 \left(r f' \rho' + 2 f \rho' + r f \rho'' \right)}{r \rho^2} - \frac{r^2 f'' + 4 r f' + 2 f - 2}{r^2 \rho}, \tag{8}$$

$$R_2 = \frac{\left(2 r \rho \rho' f' + 2 f \rho \rho' + 3 r f \rho \rho'' + r \rho^2 f'' + 2 \rho^2 f' - 3 r f \rho'^2 \right)^2}{4 r^2 \rho^6}$$
$$+ \frac{\left(r^2 f' \rho' + 4 r f \rho' + r^2 f \rho'' + 2 r \rho f' + 2 f \rho - 2\rho \right)^2}{2 r^4 \rho^4}$$
$$+ \frac{\left(2 r f' \rho' + 2 f \rho' + r \rho f'' + 2 \rho f' + r f \rho'' \right)^2}{4 r^2 \rho^4}, \tag{9}$$

$$K = \frac{15 f^2 \rho'^4}{4\rho^6} - \frac{3 f \rho'^2 \left(f' \rho' + 2 f \rho'' \right)}{\rho^5}$$
$$+ \frac{4 r f \rho' \rho'' \left(r f' + f \right) + 2 r^2 f'^2 \rho'^2 + 2 f \rho'^2 \left(r f' - r^2 f'' + 5 f - 1 \right) + 3 r^2 f^2 \rho''^2}{r^2 \rho^4}$$
$$+ \frac{2 \left[r^3 f f'' \rho'' + 2 r^2 f f' \rho'' + \rho' \left(4 r f f' - 4 f + r^3 f' f'' + 2 r^2 f'^2 + 4 f^2 \right) \right]}{r^3 \rho^3}$$
$$+ \frac{r^4 f''^2 + 4 r^2 f'^2 + 4 f^2 - 8 f + 4}{r^4 \rho^2}, \tag{10}$$

describes a static spherically symmetric black hole. In the above specific setting, ρ and v_r are constrained by the relation,[2]

$$\rho v_r = \frac{A}{r^2}, \tag{7}$$

which can be derived by integrating Eq. (2) with respect to the radial coordinate, where A is integration constant. Note that ρv_r is divergent at $r = 0$ in the manner of r^{-2}. This divergence appears at $r = 0$ in the following three cases:

where the prime denotes the derivative with respect to the radial coordinate.

Now let us analyze whether the three curvature invariants are finite or not when $r \to 0$ in the first case mentioned above. Substituting Eq. (7), i.e., $\rho = A/(r^2 v_r)$, into Eqs. (8), (9), and (10), we express explicitly the leading orders of the three curvature invariants,

$$R = \frac{2 v_0^3}{A} + O(r), \tag{11}$$

$$R_2 = \frac{2 v_0^2}{A^2} \left(v_0^4 - 2 v_0^2 + 2 \right) + O(r^2), \tag{12}$$

---

[2] This represents the peculiarity of acoustic intervals which will be utilized to pick ARBHs out.

[3] Here "finite" includes zero and nonzero constants.

$$K = \frac{4v_0^2}{A^2} \left(v_0^4 - 2v_0^2 + 2 \right) + O(r^2), \qquad (13)$$

where $v_0 \equiv \lim_{r \to 0} v_r$. They are obviously finite as r goes to zero. As to the asymptotic behaviors of ρ at $r \to 0$, we know from Eq. (7), $\rho(r) \sim 1/r^{2+a}$ with $a \geq 0$, where $a > 0$ corresponds to that v_r goes to zero in the manner of r^a and $a = 0$ corresponds to that v_0 is a nonzero constant. Moreover, we have to require the asymptotic flatness of the metric (Eq. (6) associated with Eq. (7)) in the first case. Let us analyze the leading orders of $v_r(r)$ and $\rho(r)$. If $v_r(r) \to A/r^2$ and $\rho(r) \to 1$ when $r \to \infty$, the asymptotic flatness is ensured. As a result, the models constructed in the first case can be regarded as a candidate of ARBHs.[4]

For the second case in which ρ is finite, while v_r is divergent at $r = 0$, we can judge by following the way for the first case that the three curvature invariants are divergent as r goes to zero. In fact, we have a shortcut to reach the goal. If we choose the asymptotic behaviors of ρ and v_r, for instance, to be $\rho(r) \sim 1$ and $v_r(r) \sim A/r^2$ as $r \to 0$, respectively, the shape function of Eq. (6) tends to $1 - A^2/r^4$, which definitely describes a singular spacetime. Thus, no ARBHs can be given in the second case.

As to the third case where both ρ and v_r are divergent as $r \to 0$, we can easily determine from Eqs. (8)–(10) that no ARBHs can be constructed in this case, either.

In summary, Eq. (6) associated with Eq. (7) indeed describes an ARBH when the fluid density is divergent while the radial velocity is finite at $r = 0$, where the fluid density plays the role of a conformal factor, see footnote 4 for a detailed explanation.

2.2 Completeness of geodesics

To check the geodesic completeness of the metric Eq. (6), we start with the Lagrangian [34] of a test particle constrained in the equatorial orbit $\theta = \pi/2$,

$$2\mathscr{L} = \rho \left(f \dot{t}^2 - \frac{\dot{r}^2}{f} - r^2 \dot{\phi}^2 \right), \qquad (14)$$

where the dot stands for the derivative with respect to affine parameter τ. Since t and ϕ are cyclic coordinates, one has two integrations of motion,

$$P_t = f\rho \dot{t} \equiv \mathbb{E}, \qquad P_\phi = -r^2 \rho \dot{\phi} \equiv -\mathbb{L}, \qquad (15)$$

where the energy $\mathbb{E}$ and angular momentum $\mathbb{L}$ are conserved quantities for a free radially infalling particle in static spacetimes. Then replacing the velocities in Eq. (14) by Eq. (15)

we obtain

$$\dot{r}^2 = V_{\text{eff}}, \qquad V_{\text{eff}} = \frac{\mathbb{E}^2}{\rho^2} - \frac{\mathbb{L}^2 f}{r^2 \rho^2} - \delta \frac{f}{\rho}, \qquad (16)$$

where $\delta = 0$ corresponds to null and $\delta = 1$ to timelike geodesics, respectively. For simplicity, we consider the radial geodesic motion, which implies that the angular momentum vanishes, $\mathbb{L} = 0$. Now we can write down the affine parameter by the following integral,

$$\tau = \int_{r_f}^{r_i} \frac{dr}{\sqrt{V_{\text{eff}}}}, \qquad (17)$$

where r_i and r_f represent the initial and final positions, respectively.

For a null geodesic, $\delta = 0$, the integrand of Eq. (17) can be written as follows:

$$\frac{1}{\sqrt{V_{\text{eff}}}} = \frac{\rho}{\mathbb{E}}. \qquad (18)$$

Since ρ diverges at $r = 0$, Eq. (18) implies that the proper time is also divergent.

For a timelike geodesic, $\delta = 1$, the integrand can be written as

$$\frac{1}{\sqrt{V_{\text{eff}}}} = \frac{\rho}{\sqrt{\mathbb{E}^2 - f\rho}}. \qquad (19)$$

From Eq. (16), we deduce that $\mathbb{E}^2 - f\rho \geqslant 0$, which means that $\mathbb{E}$ goes to infinity if $f > 0$ inside the innermost horizon. That is to say, the test particle needs infinite energy to reach the center of ARBHs, so there are no particles that can reach the center. Alternatively, considering that $f < 0$ inside horizons and $\mathbb{E}$ is finite but ρ goes to infinity when $r \to 0$, we have $1/\sqrt{V_{\text{eff}}} \to \sqrt{\rho}/\sqrt{-f}$. Thus, the integrand is also divergent, i.e., the timelike geodesic is complete as well.

As a matter of fact, Eq. (16) describes a particle that is moving in a negative potential well but has vanishing total energy. Intuitively, this test particle cannot reach the center of ARBHs within finite "time" because V_{eff} vanishes at $r = 0$.

In this section, we have proven that the Ricci scalar R, the contraction of two Ricci tensors R_2, and the Kretschmann scalar K are finite at $r = 0$, and both the null and timelike geodesics are complete in the ARBH spacetimes, which means that the ARBHs we constructed have no spacetime singularity.

3 A specific model

A direct way to construct a RBH is to substitute a shape function into Eq. (6), which is similar to the case of Schwarzschild BHs, then one can determine ρ and the metric $g_{\mu\nu}$ with the help of Eq. (7). Nevertheless, such a RBH is the lack of asymptotic flatness. Therefore, considering the asymptotic behaviors of the fluid density at zero and at infinity together

---

[4] We note that the density ρ can indeed be regarded as a conformal factor due to its asymptotic behaviors: $\rho(r) \sim 1/r^{2+a}$ at zero and $\rho(r) \sim 1$ at infinity. Based on such asymptotic behaviors, one of the possible forms reads, $\rho(r) = \left(1 + \frac{L^2}{r^2} \right)^{2b}$, where $b \equiv \frac{2+a}{4}$ and $L \equiv A^{1/(4b)}$, see, for instance, the conformal factors chosen in Refs. [22,36].

with the constraint between the density and the radial velocity, we give such an ARBH model,

$$\rho = \rho_* \left(1 + \frac{L^2}{r^2}\right)^{2N}, \qquad v_r = \frac{A}{\rho_* r^2 \left(1 + \frac{L^2}{r^2}\right)^{2N}}, \qquad (20)$$

where ρ_* is a constant with the dimension of density and the integration constant A has been introduced in Eq. (7). As explained in Refs. [35,36,46], L is a typical length scale of this model, such as the horizon radius or the Planck length, and N, a dimensionless constant, determines whether the scalar curvatures are regular at the center of this model. Further, we perform such a transformation,

$$r \to \sqrt{\frac{A}{\rho_*}} r, \qquad L \to \sqrt{\frac{A}{\rho_*}} L, \qquad (21)$$

in Eq. (20), and substitute the transformed Eq. (20) into the line element, Eq. (5), and then let the line element absorb ρ_*. In this way, we make the new line element look like Eq. (5) but associate with the dimensionless density and radial velocity[5] as follows:

$$\rho = \left(1 + \frac{L^2}{r^2}\right)^{2N}, \qquad v_r = \frac{1}{r^2 \left(1 + \frac{L^2}{r^2}\right)^{2N}}. \qquad (22)$$

We emphasize that the new line element is independent of the constant density ρ_* and the integration constant A but dependent only on the parameters L and N.

Now we substitute Eqs. (5), (6), and (22) into Eqs. (8)–(10) and thus derive the leading orders of curvature invariants near $r = 0$. We notice that the leading orders depend on N. When $N \le 1/2$, the leading orders near $r = 0$ are

$$R = \frac{6 - 4N(2N+1)}{L^{12N}} r^{6(2N-1)}, \qquad (23)$$

$$R_2 = \frac{8N\left[\left(4N^2(6N-17) + 86N\right) - 51\right] + 90}{L^{24N}} r^{12(2N-1)}, \quad (24)$$

$$K = \frac{16N\left[\left(4N^2(27N-76) + 329N\right) - 160\right] + 468}{L^{24N}} r^{12(2N-1)}; \quad (25)$$

when $N > 1/2$, they have the following forms,

$$R = \frac{12(1-2N)N}{L^{4N}} r^{2(2N-1)}, \qquad (26)$$

$$R_2 = \frac{16N^2[2N(6N-7) + 5]}{L^{8N}} r^{4(2N-1)}, \qquad (27)$$

$$K = \frac{16N^2[4N(3N-4) + 7]}{L^{8N}} r^{4(2N-1)}. \qquad (28)$$

From Eqs. (23)–(28), we can confirm that the curvature invariants are finite when $N \ge 1/2$.

---

[5] Due to the setting, $c = 1$, the radial velocity is dimensionless, which gives rise to the dimensionless length and new line element in our units.

To illustrate the finiteness of curvature invariants and completeness of geodesics for the specific model, we take two different cases, $N = 1/2$ and $N = 1$, where the former is critical while the latter is a sample of $N > 1/2$.

- (i) $N = 1/2$. In this case, there exists only one horizon whose radius equals $r_+ = \sqrt{1 - L^2}$, where the existence of horizons requires $L^2 < 1$. Eq. (22) reduces to

$$\rho = 1 + \frac{L^2}{r^2}, \qquad v_r = \frac{1}{r^2 + L^2}. \qquad (29)$$

Correspondingly, the leading orders of the three curvature invariants near $r = 0$ read

$$R = \frac{2}{L^6} + O(r^2), \qquad R_2 = \frac{4L^8 - 4L^4 + 2}{L^{12}} + O(r^2),$$

$$K = \frac{8L^8 - 8L^4 + 4}{L^{12}} + O(r^2). \qquad (30)$$

They are obviously finite. As to the completeness of geodesics, for the null geodesics with $\delta = 0$, substituting Eq. (29) into Eqs. (17) and (18), we obtain the affine parameter,

$$\tau = \frac{1}{\mathbb{E}} \left(r_i - r_f - \frac{L^2}{r_i} + \frac{L^2}{r_f}\right), \qquad (31)$$

which goes to infinity when the initial position is fixed and the final position goes to zero. Moreover, for the time-like geodesics with $\delta = 1$, Eq. (17) cannot be expressed analytically because of the complicated integrand, but the expansion of the integrand near $r = 0$ can be written as

$$\frac{1}{\sqrt{V_{\text{eff}}}} = \frac{L^3}{\sqrt{(1 - L^4)}} \frac{1}{r} + O(r), \qquad (32)$$

which implies that the affine parameter diverges when the final position goes to zero.

- (ii) $N = 1$. For this case, the horizon radii are $r_\pm = \sqrt{(1 - 2L^2)/2 \pm \sqrt{1 - 4L^2}/2}$, where "+" means the outer horizon and "−" the inner horizon, and the existence of horizons gives the condition, $L^2 \le 1/4$. Eq. (22) gives the density and radial velocity as follows:

$$\rho = \left(1 + \frac{L^2}{r^2}\right)^2, \qquad v_r = \frac{1}{r^2 \left(1 + \frac{L^2}{r^2}\right)^2}, \qquad (33)$$

and thus the expansions of curvature invariants near $r = 0$ read

$$R = -\frac{12}{L^4} r^2 + O(r^4), \qquad R_2 = \frac{48}{L^8} r^4 + O(r^6),$$

$$K = \frac{48}{L^8} r^4 + O(r^6). \qquad (34)$$

It is obvious that the curvature invariants converge at $r = 0$. For the completeness of the null geodesics with $\delta = 0$, we derive the affine parameter,

$$\tau = \frac{1}{\mathbb{E}} \left(\frac{L^4 + 6L^2 r_f^2 - 3r_f^4}{3r_f^3} - \frac{L^4 + 6L^2 r_i^2 - 3r_i^4}{3r_i^3} \right),$$
(35)

which is divergent when $r_f \to 0$, i.e., the particles moving along the radial geodesic can never reach the center within a finite proper time. For the completeness of the timelike geodesics with $\delta = 1$, we give the expansion of the integrand of Eq. (17) near $r = 0$,

$$\frac{1}{\sqrt{V_{\text{eff}}}} = \frac{L^2}{r^2} + O(r^2),$$
(36)

which diverges at $r = 0$ as expected.

Now we illustrate the regularity of this specific ARBH model in four figures. We plot the graphs of shape function $f(r)$ in Fig. 1 for the cases of $N = 1/2$ and $N = 1$. The three curvature invariants as a function of the radial coordinate are plotted in Fig. 2 for the case of $N = 1/2$ and in Fig. 3 for the case of $N = 1$ according to Eqs. (8)–(10) and Eqs. (29) and (33). Moreover, we plot the graph of the affine parameter of null geodesics as a function of the final position in Fig. 4 according to Eqs. (31) and (35).

4 Potentials of external driving force

Our approach to construct the acoustic metric in Sect. 3 is based on the following assumptions:

- The speed of sound is a position-independent constant and can be normalized to unity, $c = 1$;
- The fluid is irrotational, i.e., its vorticity w vanishes, $w \equiv \nabla \times \boldsymbol{v} = 0$;
- The fluid is spherically symmetric, i.e., the velocity $\boldsymbol{v}$ has only radial component v_r and all physical quantities, such as ρ, v_r, etc., depend only on radial coordinate r.

Therefore, if Euler's equation Eq. (3) did not involve an external-force term, the above items would lead to a problem on consistency when we are going to establish the acoustic counterpart of a gravitational metric. On the premise of the above three assumptions, the continuity equation and Euler equation are reduced to

$$\partial_r \left(r^2 \rho v_r \right) = 0,$$
(37)

and

$$\partial_r \left(\frac{v_r^2}{2} \right) + \partial_r \ln(\rho) = -\partial_r \psi,$$
(38)

respectively. Thus, if there were no the external-force term, $-\partial_r \psi$, one would fix v_r (or ρ) via the continuity equation when ρ (or v_r) is given to mimic a gravitational metric, but such a treatment would probably contradict to the Euler equation. In other words, we have actually only one unknown variable v_r (or ρ) but two dynamical equations, i.e., one redundant condition appears. Nonetheless, this case will never happen when the external-force potential exists.

Now we calculate the external potential for our ARBH model established in Sect. 3. The first integral of Euler's equation in Eq. (38) provides

$$\psi = \psi_0 - \ln(\rho) - \frac{v_r^2}{2},$$
(39)

where ψ_0 is an integration constant. Then, substituting Eq. (22) into Eq. (39), we arrive at

$$\psi = \psi_0 - 2N \ln \left(1 + \frac{L^2}{r^2} \right) - \frac{1}{2r^4 \left(1 + \frac{L^2}{r^2} \right)^{4N}},$$
(40)

whose asymptotic behaviors at $r \to 0$ and $r \to \infty$ take the forms,

$$\psi \xrightarrow{r \to 0} 4N \ln(r), \qquad \psi \xrightarrow{r \to \infty} \psi_0 - 2N \frac{L^2}{r^2},$$
(41)

respectively. In other words, the external force is asymptotic to $-4N/r$ around the center and vanishes at infinity. It is obvious that the Euler equation of our ARBH model, Eq. (39), has a consistent asymptotic behavior when v_r is finite and ρ divergent as $r \to 0$.

Because the external-force term in Euler's equation does not affect [3] acoustic metrics, so it has rarely been drawn much attention [8]. As we have discussed above, this term suggests a way to realize the specific fluid when we study the acoustic analogue of an astronomical black hole, so it is critical.

5 Energy conditions

As is known, the energy conditions can examine cosmological models and strong gravitational fields, and give restrictions on the forms of energy–momentum tensors of matter fields. In general, the energy conditions are classified [37] into four categories: Null energy condition (NEC), weak energy condition (WEC), strong energy condition (SEC), and dominant energy condition (DEC).

Based on Refs. [35,38], we briefly explain the meanings of the four energy conditions. The NEC requires that both
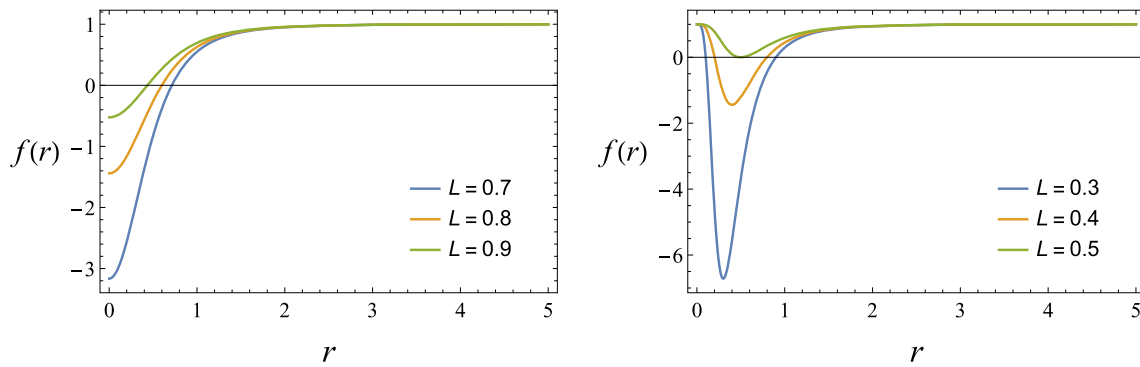
Fig. 1 $f(r)$ with respect to r for the cases of $N = 1/2$ (left) and $N = 1$ (right), only one horizon in the former case but normally two horizons in the latter. Note that the values of L satisfy $L^2 < 1$ in the left graph and $L^2 \le 1/4$ in the right graph, respectively
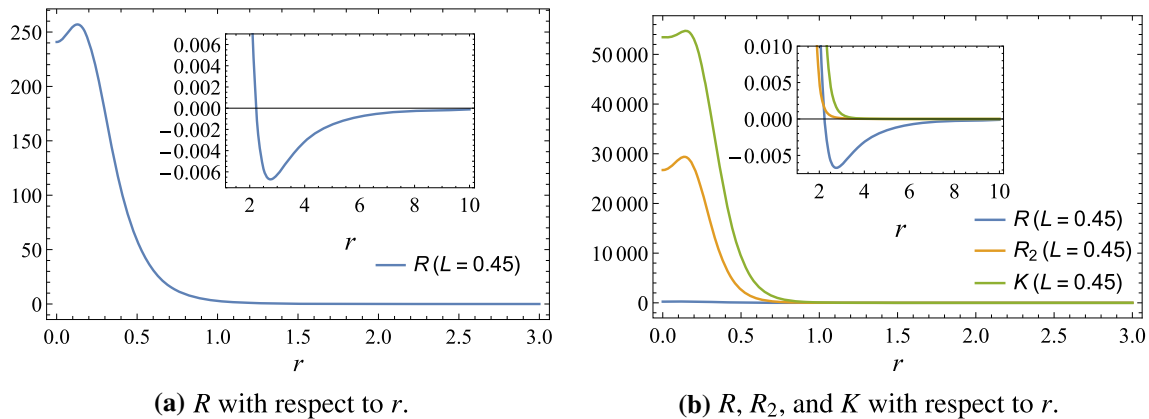

(a) R with respect to r.

(b) R, R_2, and K with respect to r.

Fig. 2 R, R_2, and K with respect to r for the case of $N = 1/2$, where $L = 0.45$ which satisfies $L^2 < 1$. Note that R is separated from the right graph and presented in the left graph in order to show its detail features
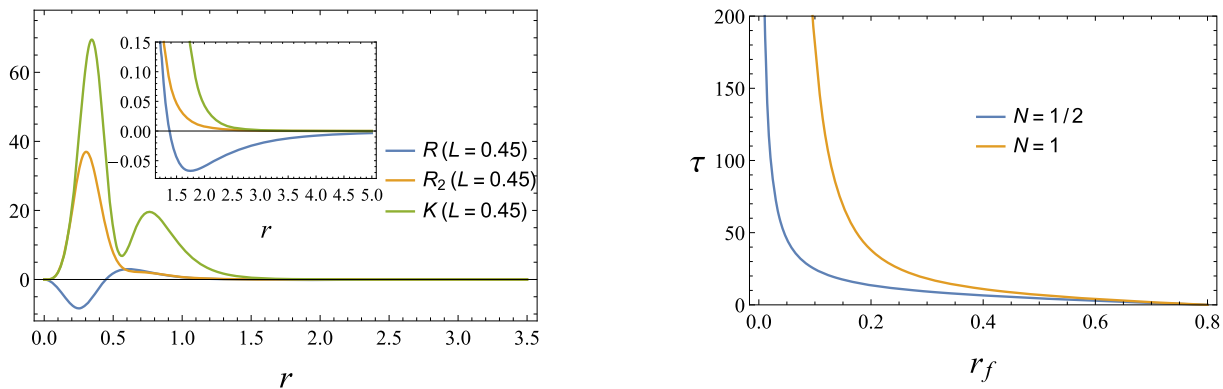
Fig. 3 R, R_2, and K with respect to r for the case of $N = 1$, where $L = 0.45$ which satisfies $L^2 \le 1/4$

Fig. 4 τ with respect to r_f for the two cases of $N = 1/2$ and $N = 1$, where $L = 0.45$, the initial position $r_i = 0.8$, and energy $\mathbb{E} = 0.1$

energy density and pressure cannot be negative when measured by an observer traversing a null curve, or if one of them is negative, the other must be positive and its magnitude must be larger than the absolute value of the negative quantity. The WEC states that the energy density of any matter distribution measured by any observer traversing a timelike curve must

be nonnegative. The SEC requires

$$\left(T_{\mu\nu} - \frac{1}{2} T g_{\mu\nu} \right) v^\mu v^\nu \ge 0, \tag{42}$$

where v^μ is future-directed, normalized, and timelike vector, $T_{\mu\nu}$ is energy–momentum tensor, and $T = g^{\mu\nu} T_{\mu\nu}$. The DEC states that the energy flow cannot be faster than

the speed of light, i.e., it ensures the causality. The energy–momentum tensor can be written as $T^\mu_{\;\nu} \equiv g^{\mu\alpha}T_{\alpha\nu} = \text{diag}\{-\rho_0, P_1, P_2, P_3\}$, see Appendix A for the derivation and discussion. Thus, the four energy conditions can be expressed in terms of the components of the energy–momentum tensor as follows:

$$
\begin{aligned}
&\text{NEC:} \quad \rho_0 + P_i \geq 0, \quad i = 1, 2, 3,\\[4pt]
&\text{WEC:} \quad \rho_0 \geq 0, \quad \rho_0 + P_i \geq 0, \quad i = 1, 2, 3,\\[4pt]
&\text{SEC:} \quad \rho_0 + \sum_{i=1}^{3} P_i \geq 0, \quad \rho_0 + P_i \geq 0, \quad i = 1, 2, 3,\\[4pt]
&\text{DEC:} \quad \rho_0 \geq 0, \quad \rho_0 - |P_i| \geq 0, \quad i = 1, 2, 3.
\end{aligned}
\tag{43}
$$

5.1 Energy conditions of our ARBH model

Let us investigate various energy conditions for the ARBH model we just constructed. We suppose the energy–momentum tensor is proportional to the Einstein tensor of the acoustic gravity because our strategy is to investigate the physicality of a gravitational BH equivalent to our ARBH, and therefore derive the four components of $T^\mu_{\;\nu}$. Using Eqs. (6) and (7) together with Eq. (29) for the case of $N = 1/2$ or Eq. (33) for the case of $N = 1$, we can verify the relation,[6] $P_2 = P_3$, so there are only six independent inequalities in Eq. (43) that are listed below.

For the case of $N = 1/2$, we compute the six independent quantities,

The energy conditions require that these quantities should be nonnegative. We plot the allowed regions on the $r - L$ plane in Fig. 5.

Combining the six subfigures in Fig. 5 with the four energy conditions in Eq. (43), we can determine the domains that the energy conditions are satisfied for the case of $N = 1/2$, which is plotted in Fig. 6.

We can see from Fig. 6 that the SEC is completely violated in the entire parameter range and spacetime, $L^2 < 1$ and $r \in [0, \infty)$. This is actually what we expected because the spacetime with $f = 1 - 1/r^4$ is asymptotic to the metric of our ARBH model, see Eqs. (6) and (29) in the limit of $r \gg L$, and such a spacetime is of repulsive interaction which breaks the SEC, see Appendix B for a detailed explanation. However, the situation of our ARBH model is more complicated than usual. We see in Fig. 5d that $\rho_0 + \sum_{i=1}^{3} P_i \geqslant 0$ is satisfied in one region outside the horizon, i.e., the ARBH produces an attractive interaction outside the horizon although the SEC is violated based on Ref. [47]. The reason that makes the SEC invalid is that $\rho_0 + P_1 \geq 0$ is violated outside the horizon, which is different from the situation in the usual BH models with $f = 1 - 1/r^4$. In addition, the NEC, WEC, and DEC are satisfied in a piece of domains inside the horizon (also including the horizon as boundary) for the parameter range $0.8 < L \leq 1.0$.

For the case of $N = 1$, we compute the six independent quantities,

$$
\rho_0 = \frac{L^8 - 3(L^4 + 1)r^4 - 2L^2 r^6 + 4L^2 r^2}{8\pi (L^2 + r^2)^5},
\tag{44}
$$

$$
\rho_0 + P_1 = -\frac{6L^2 r^2 \left[(L^2 + r^2)^2 - 1\right]}{8\pi (L^2 + r^2)^5},
\tag{45}
$$

$$
\rho_0 + P_2 = \frac{2L^8 + 6L^6 r^2 + L^4(6r^4 - 1) + 2L^2 r^2(r^4 - 1) - 9r^4}{8\pi (L^2 + r^2)^5},
\tag{46}
$$

$$
\rho_0 + \sum_{i=1}^{3} P_i = \frac{2L^8 + 6L^6 r^2 + 2L^4(3r^4 - 1) + 2L^2 r^2(r^4 - 3) - 12r^4}{8\pi (L^2 + r^2)^5},
\tag{47}
$$

$$
\rho_0 - |P_1| = \frac{L^8 - 3(L^4 + 1)r^4 - 2L^2 r^6 + 4L^2 r^2}{8\pi (L^2 + r^2)^5} - \left| \frac{L^8 + 3(3L^4 - 1)r^4 + 4L^2 r^6 + 2(3L^4 - 1)L^2 r^2}{8\pi (L^2 + r^2)^5} \right|,
\tag{48}
$$

$$
\rho_0 - |P_2| = \frac{L^8 - 3(L^4 + 1)r^4 - 2L^2 r^6 + 4L^2 r^2}{8\pi (L^2 + r^2)^5} - \left| \frac{L^8 + 6L^6 r^2 + L^4(9r^4 - 1) + L^2(4r^6 - 6r^2) - 6r^4}{8\pi (L^2 + r^2)^5} \right|.
\tag{49}
$$

---

[6] In fact, this condition is valid for a general static and spherically symmetric BH.

$$\rho_0 = -\frac{r^4\left[4L^{10} + (16L^4 + 3)r^6 + (16L^4 + 3)L^4 r^2 + 4L^2 r^8 + 2(12L^4 - 7)L^2 r^4\right]}{8\pi(L^2 + r^2)^8}, \tag{50}$$

$$\rho_0 + P_1 = \frac{4L^2 r^2(L^2 + r^2 - r)(L^2 - 3r^2)(L^2 + r^2 + r)[(L^2 + r^2)^2 + r^2]}{8\pi(L^2 + r^2)^8}, \tag{51}$$

$$\rho_0 + P_2 = \frac{r^2\left[4L^{12} + 20L^{10}r^2 + (20L^4 - 9)r^8 + (40L^4 - 1)L^4 r^4 + 4L^2 r^{10} + 2(20L^4 + 7)L^2 r^6\right]}{8\pi(L^2 + r^2)^8}, \tag{52}$$

$$\rho_0 + \sum_{i=1}^{3} P_i = \frac{4r^2\left[3L^{12} + 13L^{10}r^2 + 22L^8 r^4 + 18L^6 r^6 + 7L^4 r^8 + L^2 r^6(r^4 + 3) - 3r^8\right]}{8\pi(L^2 + r^2)^8}, \tag{53}$$

$$\rho_0 - |P_1| = -\frac{r^4\left[4L^{10} + (16L^4 + 3)r^6 + (16L^4 + 3)L^4 r^2 + 4L^2 r^8 + 2(12L^4 - 7)L^2 r^4\right]}{8\pi(L^2 + r^2)^8}$$
$$- \left|\frac{r^2\left[-4L^{12} - 8L^{10}r^2 + 8L^8 r^4 + 32L^6 r^6 + L^4(28r^8 + r^4) + 2L^2(4r^{10} + r^6) - 3r^8\right]}{8\pi(L^2 + r^2)^8}\right|, \tag{54}$$

$$\rho_0 - |P_2| = -\frac{r^4\left[4L^{10} + (16L^4 + 3)r^6 + (16L^4 + 3)L^4 r^2 + 4L^2 r^8 + 2(12L^4 - 7)L^2 r^4\right]}{8\pi(L^2 + r^2)^8}$$
$$- \left|\frac{2r^2\left[2L^{12} + 12L^{10}r^2 + 32L^6 r^6 + 3(6L^4 - 1)r^8 + (28L^4 + 1)L^4 r^4 + 4L^2 r^{10}\right]}{8\pi(L^2 + r^2)^8}\right|. \tag{55}$$

The energy conditions require that these quantities should be nonnegative. We plot the allowed regions on the $r - L$ plane in Fig. 7. Similarly, the corresponding valid domains of energy conditions are shown in Fig. 8 for the case of $N = 1$ when Fig. 7 is combined with Eq. (43).

We can see from Fig. 8 that the NEC and SEC are satisfied in two pieces of domains for the parameter range $0 < L \leq 1/2$, where one is located inside the inner horizon and the other between the inner and outer horizons (also including the horizons as boundaries). It is worthy to emphasize that the situation of SEC in our model is a counterexample of the work [48] in which the breaking domain of SEC for a regular black hole with metric $g_{\mu\nu} = \text{diag}\left\{-f, f^{-1}, r^2, r^2\sin^2\theta\right\}$ must be located inside horizon. The reason is that our ARBH model does not satisfy the simple relation, $-g_{tt}g_{rr} = 1$. Therefore, our situation of SEC becomes complicated. Moreover, the WEC and DEC are satisfied in only one piece of domains between the inner and outer horizons (also including the two horizons as boundaries for WEC and only the outer horizon as boundary for DEC) for the parameter ranges $0 < L \leq 1/2$ (WEC) and $0 < L < 1/2$ (DEC), respectively.

Besides the above discussions of energy conditions on the $r - L$ plane, for our ARBH model depicted by Eq. (22), we further investigate its energy conditions by plotting the valid domains on the $r - N$ plane in Fig. 9c. The NEC, WEC and SEC are satisfied in two pieces of domains for the parameter range $1/2 < N \leq 1$ and $L = 1/2$, where one piece is located inside the inner horizon and the other between the inner and outer horizons (also including the horizons as boundaries). However, the DEC is satisfied in only one piece of domains between the inner and outer horizons (also including the outer

horizon as boundary) for the parameter range $1/2 < N < 1$ and $L = 1/2$. In particular, Fig. 9c shows that the SEC is completely violated in the entire spacetime $r \in [0, \infty)$ in the vicinity of $N = 1/2$.

5.2 Energy conditions of conformally related Schwarzschild black holes

In Sects. 2 and 3, we have seen that our ARBH model can be regarded as a conformally related BH in the perspective of finiteness of curvature invariants and completeness of geodesics, where the density of fluid acts as the scale factor. It is just a seeming reason that the line element of our ARBH model, Eq. (5) and Eq. (22), looks like that of a conformally related BH. The virtual reason is that the acoustic analog leads to a non-vanishing partition function if it is interpreted in the context of conformally invariant theory. Let us extend this discussion. If the Euclidean action of our ARBH model were constructed [49] by

$$\tilde{I} = \int \mathrm{d}x^4 \sqrt{-g}\, R + \cdots, \tag{56}$$

where the ellipsis represents the surface term and matter sectors, it would be divergent since $\sqrt{-g}$ is divergent at $r = 0$. As a result, all the thermodynamic variables computed by the path-integral method would be trivial because the partition function $Z = e^{-\tilde{I}}$ vanishes. Nevertheless, if we construct our ARBH model in the conformal theory [50], i.e.,

$$I = \int \mathrm{d}x^4 \sqrt{-g}\left[\frac{1}{12}\varphi^2 R - \frac{1}{2}\varphi g^{\mu\nu}\nabla_\mu \nabla_\nu \varphi\right] + \cdots, \tag{57}$$

(a) $\rho_0 \geq 0$

(b) $\rho_0 + P_1 \geq 0$

(c) $\rho_0 + P_2 \geq 0$

(d) $\rho_0 + \sum_{i=1}^{3} P_i \geq 0$

(e) $\rho_0 - |P_1| \geq 0$
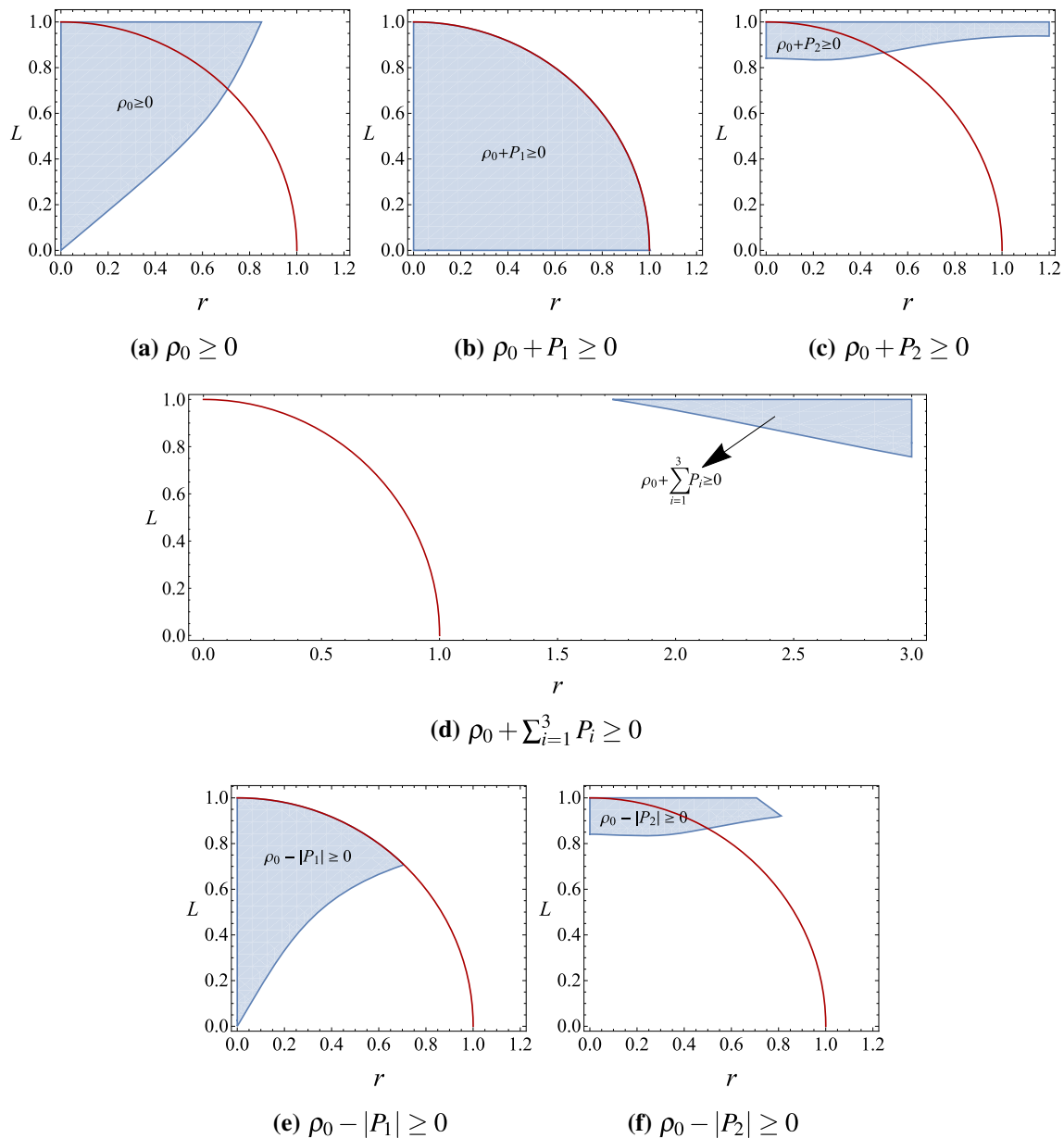
(f) $\rho_0 - |P_2| \geq 0$

Fig. 5 The blue shadows show the physical regions in which the corresponding inequalities are satisfied for the case of $N = 1/2$, where the red curves are horizons. Note that the existence of horizons gives the constraint, $L^2 < 1$, in this case

where φ is a massless scalar field and ∇_μ covariant derivative, the situation will be improved because the scalar field φ can absorb the divergence of the measure $\sqrt{-g}$ based on the conformal symmetry.

Here we intend to emphasize that this analogue BH has its own specific properties in the energy conditions that are distinct from those of a conformally related BH. We shall take CRSBHs as an example, analyze its energy conditions and compare them with our ARBH model's.

The scale factor of CRSBHs takes [22] the form,

$$S(r) = \left(1 + \frac{\bar{L}^2}{r^2}\right)^{2\bar{N}}, \tag{58}$$

where $\bar{N}$ and $\bar{L}$ have the same meanings as those of N and L in Eq. (22), and $\bar{L}$ and $\bar{N}$ are independent of each other but L and N are related to each other due to the existence of horizons. We can verify that the regularity of CRSBHs requires $\bar{N} \geqslant 3/4$.

Following the same procedure as that in the above subsection, we plot the valid domains of energy conditions of

Fig. 6 The blue shadows show the valid domains of NEC, WEC, and DEC for the case of $N = 1/2$, where no valid domains exist for the SEC. The red curves are horizons in this case

(a) Null energy condition

(b) Weak energy condition

(c) Strong energy condition

(d) Dominant energy condition
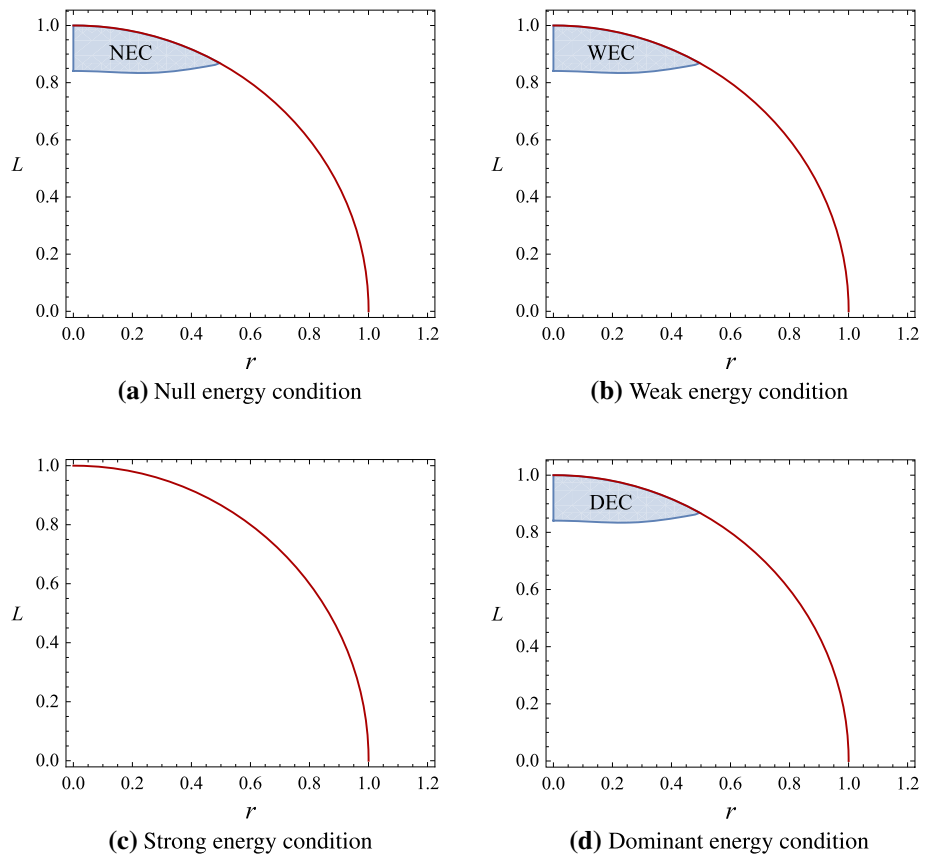
CRSBHs[7] on the $r - \bar{L}$ plane in Figs. 10 and 11 for the two cases of $\bar{N} = 3/4$ and $\bar{N} = 1$, respectively. We can see that the energy conditions are satisfied only outside the horizon of CRSBHs, which is completely different from the situation of our ARBH model in Figs. 6 and 8. We also notice that the valid domains in Figs. 10 and 11 are located in the areas with a minimum value of $\bar{L}$, and that they expand when $\bar{L}$ increases. However, it is obvious that the expansion of domains does not happen in our ARBH model, see Figs. 6 and 8, because L is constrained by the value of N. Especially, the NEC and SEC are satisfied at $r = 0$ for our ARBH model, see Figs. 8 and 9, which does not appear in the CRSBHs. This feature (the SEC is not violated at $r = 0$) implies that the interaction is attractive in the vicinity of $r = 0$ in our ARBH model, which presents the characteristic of this acoustic analog.

In addition, we plot the valid domains of energy conditions of CRSBHs on the $r - \bar{N}$ plane in Fig. 12. When comparing it with Fig. 9, we find that the domains of energy conditions of CRSBHs are located outside the horizon while those of our ARBH model inside the outer horizon. This is the main difference between the ARBHs and CRSBHs in the energy conditions, and the other differences are similar to those mentioned above between $r - L$ and $r - \bar{L}$ graphs.

---

[7] The energy conditions of CRSBHs were analyzed in Ref. [35] in which the sign of energy density is wrong. See Appendix A for our explanations.

6 Quasinormal modes of acoustic regular black holes

In this section, we discuss the sound propagation in the spacetime of our ARBH model. As mentioned in Introduction, the equation of motion for an acoustic disturbance is identical [2] to the d'Alembertian equation of a massless scalar field propagating in a curved spacetime. That is, the sound propagation in our ARBH spacetime manifests as the propagation of a massless scalar field in an effective curved spacetime, which is described by the Klein–Gordon equation. As a result, we can analyze the stability of our ARBH model by computing its QNMs in terms of the WKB method [41–45], where the 6th-order WKB method is adopted in order to have the balance between precision and complexity of numerical calculations. The Klein–Gordon equation for a massless scalar field Φ in a curved spacetime can be written as

$$\frac{1}{\sqrt{-g}} \partial_\mu \left(\sqrt{-g} g^{\mu\nu} \partial_\nu \Phi \right) = 0, \tag{59}$$

where Φ represents the disturbance to the background fluid, i.e., the potential function of acoustic waves [3]. In order to separate the variables in Eq. (59), the function Φ can be chosen as

$$\Phi = \frac{1}{r\sqrt{\rho}} \Psi(r) Y_\ell^m(\theta, \phi) e^{-i\omega t}, \tag{60}$$

(a) $\rho_0 \geq 0$

(b) $\rho_0 + P_1 \geq 0$

(c) $\rho_0 + P_2 \geq 0$

(d1) $\rho_0 + \sum_{i=1}^3 P_i \geq 0$

(d2) $\rho_0 + \sum_{i=1}^3 P_i \geq 0$

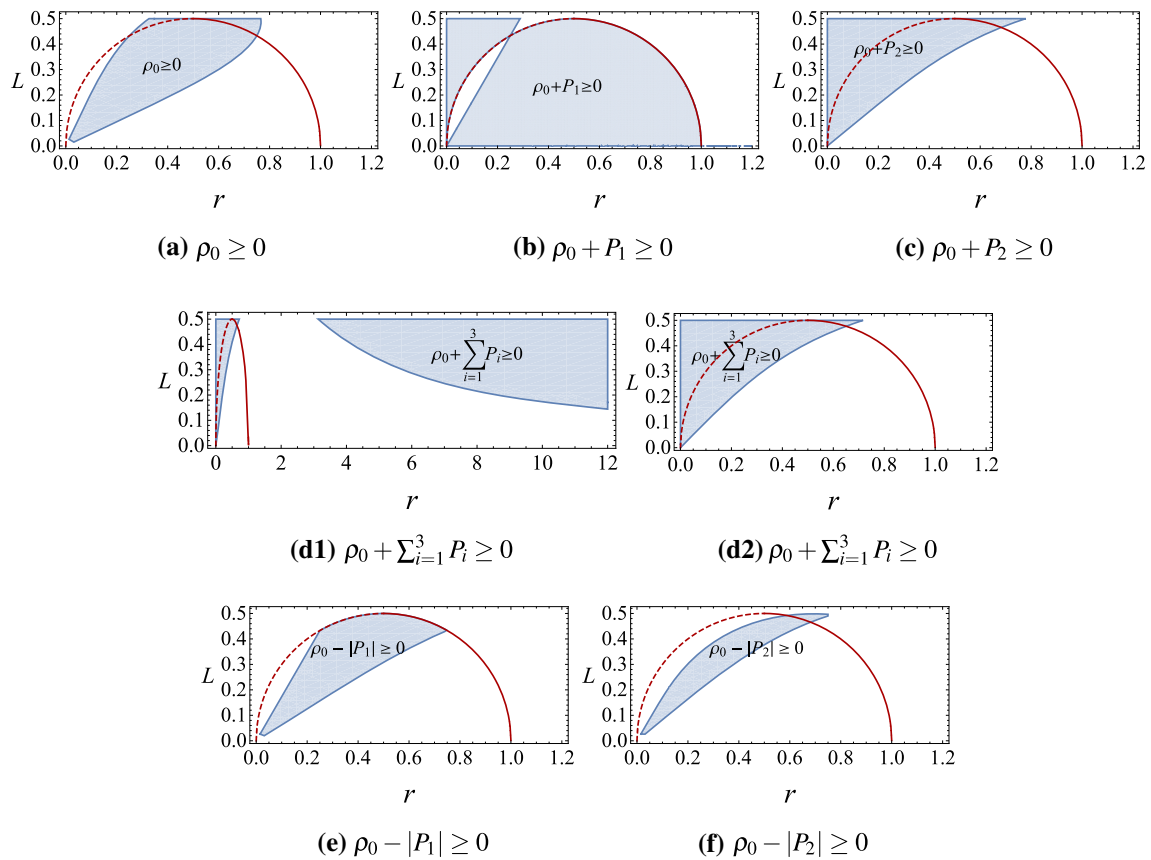**(e)** $\rho_0 - |P_1| \geq 0$

(f) $\rho_0 - |P_2| \geq 0$

Fig. 7 The blue shadows show the physical regions in which the corresponding inequalities are satisfied for the case of $N = 1$, where the dotted red curves are inner horizons while the solid ones outer horizons.

Note that the existence of horizons gives the constraint, $L^2 \leq 1/4$, in this case. Subfigure (d2) shows the detail features of the left shadow in subfigure (d1)

Fig. 8 The blue shadows show the valid domains of various energy conditions for the case of $N = 1$. The dotted red curves are inner horizons while the solid ones outer horizons in this case

(a) Null energy condition

(b) Weak energy condition

(c) Strong energy condition

(d) Dominant energy condition
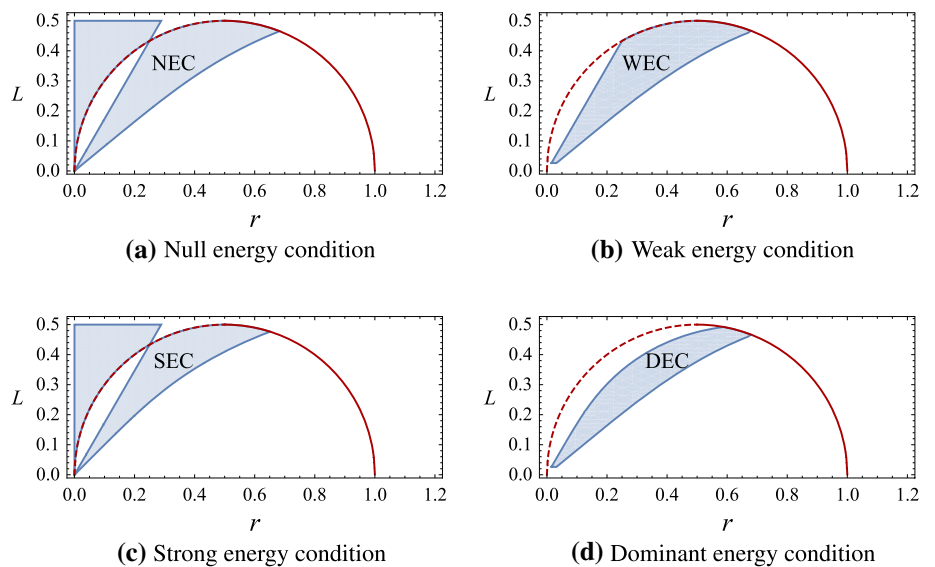
Fig. 9 The blue shadows show the valid domains of various energy conditions for the case of $L = 1/2$. The dotted red curves are inner horizons while the solid ones outer horizons in this case. The existence of horizons gives the constraint, $1/2 \leqslant N \leqslant 1$, in this case

(a) Null energy condition

(b) Weak energy condition

(c) Strong energy condition

(d) Dominant energy condition
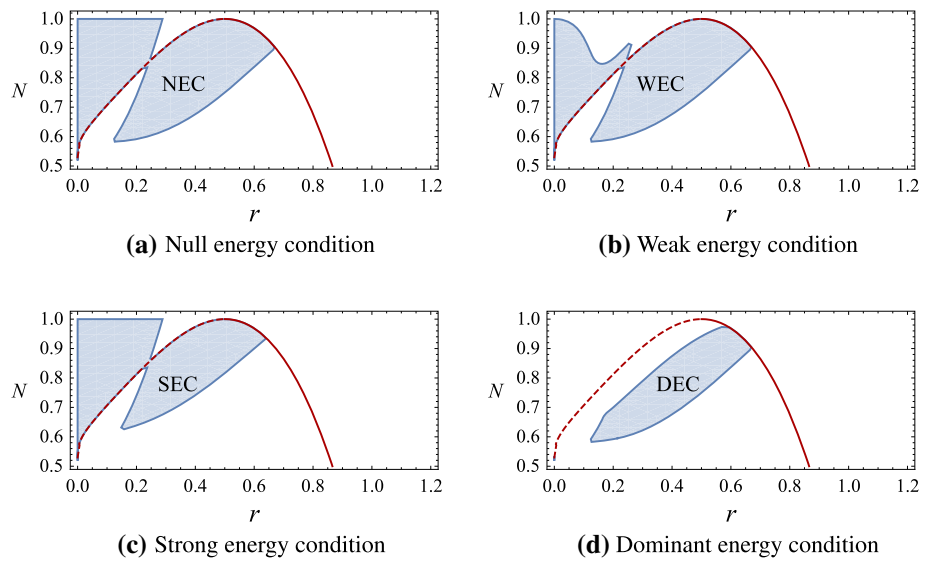
Fig. 10 The blue shadows show the valid domains of various energy conditions for the case of $\bar{N} = 3/4$. The red lines are horizons

(a) Null energy condition

(b) Weak energy condition

(c) Strong energy condition

(d) Dominant energy condition
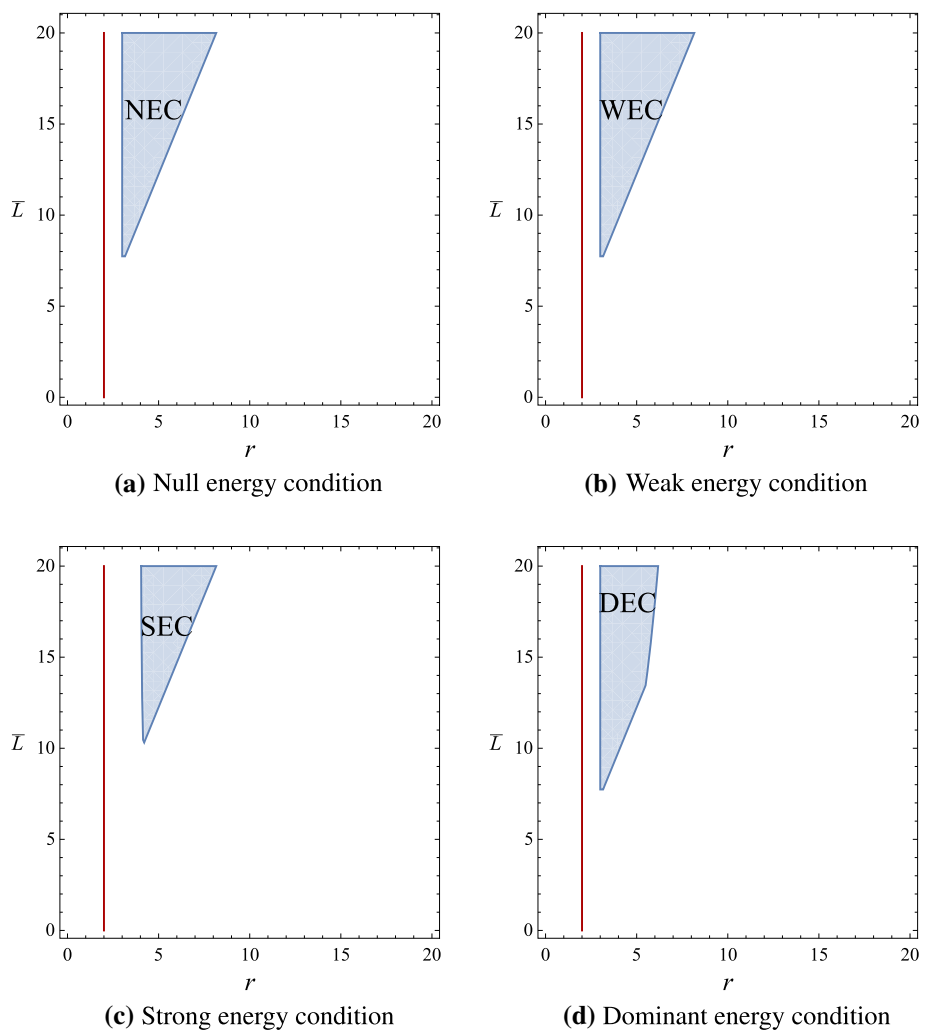
Fig. 11 The blue shadows show the valid domains of various energy conditions for the case of $\bar{N} = 1$. The red lines are horizons

(a) Null energy condition

(b) Weak energy condition

(c) Strong energy condition

(d) Dominant energy condition
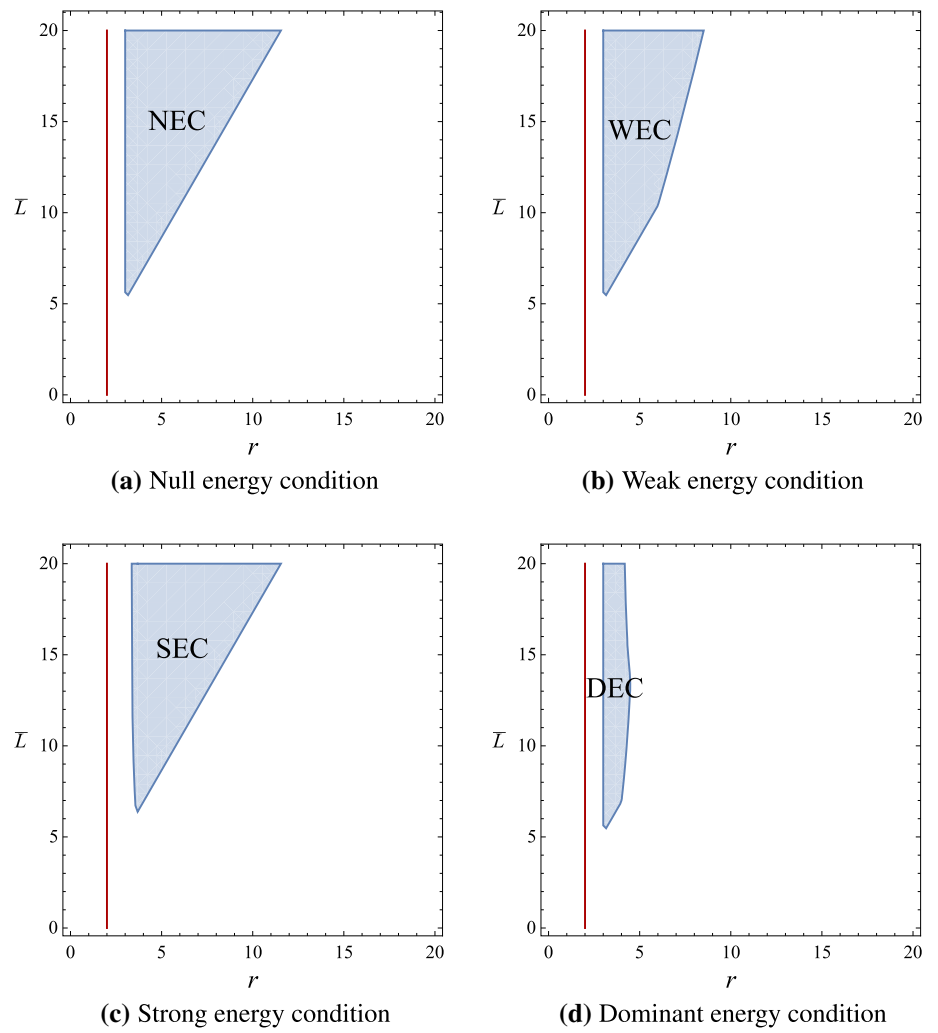
Fig. 12 The blue shadows show the valid domains of various energy conditions for the case of $\bar{L} = 10$. The red lines are horizons

(a) Null energy condition

(b) Weak energy condition

(c) Strong energy condition

(d) Dominant energy condition
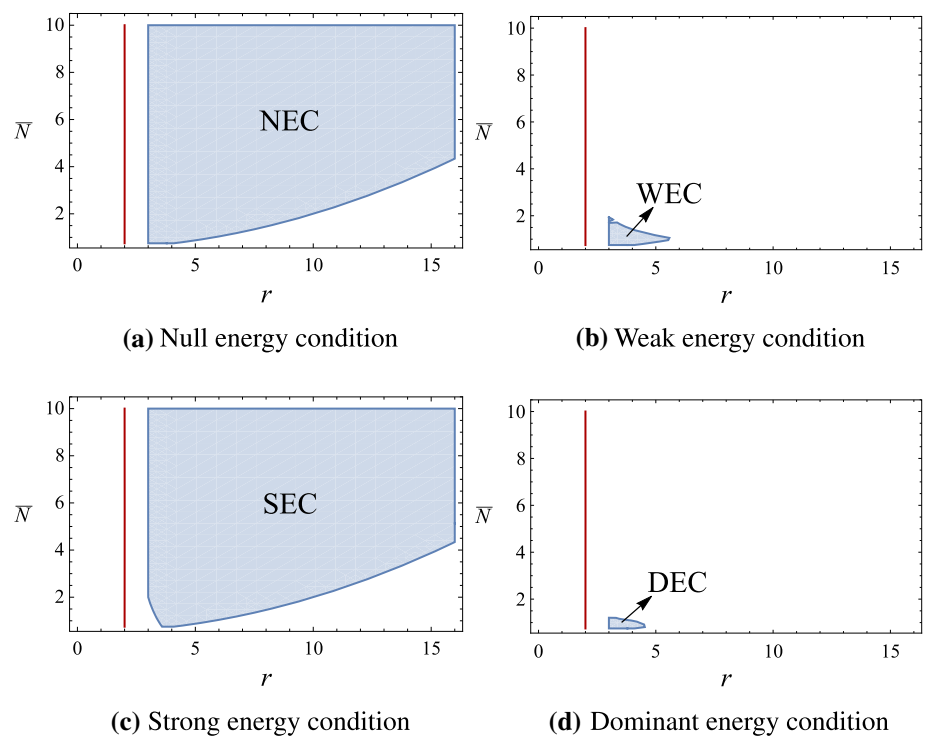
where $Y_\ell^m(\theta,\phi)$ is spherical harmonic function of degree l and order m, and l is also called the multipole number. Substituting Eq. (60) into Eq. (59), we get the Schrödinger-like equation [22],

$$\frac{d^2\Psi}{dr_*^2} + \omega^2\Psi = V(r)\Psi, \tag{61}$$

with the effective potential,

$$V(r) = f(r)\left[\frac{l(l+1)}{r^2} + \frac{1}{Z}\frac{d}{dr}\left(f(r)\frac{dZ}{dr}\right)\right], \tag{62}$$

where $Z \equiv r\sqrt{\rho}$ and r_* is the tortoise coordinate defined by $dr_* = dr/f(r)$. For our ARBH model, substituting Eq. (29) for the case of $N = 1/2$ and Eq. (33) for the case of $N = 1$ into Eq. (62), we write down explicitly the effective potentials,

$$V_{N=1/2}(r) = \left[1 - \frac{1}{(L^2+r^2)^2}\right]$$
$$\times \left[\frac{l(l+1)}{r^2} + \frac{L^2(L^2+r^2)^2 - L^2 + 4r^2}{(L^2+r^2)^4}\right], \tag{63}$$

and

$$V_{N=1}(r) = \left[1 - \frac{1}{r^4\left(1+\frac{L^2}{r^2}\right)^4}\right]$$
$$\times \left[\frac{(l+1)l}{r^2} + \frac{2(L^{12} + 5L^{10}r^2 + 10L^8r^4 + 10L^6r^6 + L^4(5r^8+r^4) + L^2r^6(r^4-5) + 2r^8)}{r^2(L^2+r^2)^6}\right]. \tag{64}$$

Now we plot the effective potential $V(r)$ with respect to radial coordinate r for different values of parameter L but a fixed $l = 10$ in Fig. 13. It can be seen that the potential has only one maximum value for the case of $N = 1/2$, while it has one minimum value and one maximum value for the case of $N = 1$. When l is fixed, both minimum and maximum values increase as L increases.

The QNMs solved from Eq. (61) together with the effective potential Eq. (62) can be cast in the complex form, $\omega = \text{Re}\,\omega + i\,\text{Im}\,\omega$, where the real part, $\text{Re}\,\omega$, represents the oscillation of perturbation, while the imaginary part, $\text{Im}\,\omega$, characterizes the dissipation of perturbation. We use the 6th-order WKB method to provide numerical solutions. It should be noted that the WKB method requires that the effective potential $V(r)$ has one single maximum outside the horizon and that the multipole number l is larger than the overtone number which is taken to be zero for the fundamental mode of scalar field perturbation [44]. We can see from Fig. 13 that our ARBH model meets the requirement.

The QNMs satisfy [45] the following formula in the 6th-order WKB method,

$$i\frac{(\omega^2 - V_0)}{\sqrt{-2V_0''}} - \sum_{i=2}^{6}\Lambda_i = n + \frac{1}{2}, \tag{65}$$

where V_0 is the maximum of the effective potential $V(r)$, $V_0'' = \left.\frac{d^2V(r)}{dr_*^2}\right|_{r_*=(r_*)_0}$, r_0 is the position of the peak value of the effective potential, n is overtone number, and Λ_i $(i = 2, 3, \ldots, 6)$ are constant coefficients related to the corrections from the 2nd- to 6th-orders. By substituting Eq. (63) or Eq. (64) into Eq. (65), we can obtain the QNMs numerically for our ARBH model in the case of $N = 1/2$ or $N = 1$.

In Fig. 14, we show the results of the QNMs depending on the characteristic parameter l, where $L = 0.45$ and $n = 0$ are set. The left diagram of Fig. 14 correspond to the change of $\text{Re}\,\omega$ with respect to l for the cases of $N = 1/2$ and $N = 1$, respectively, and the right diagram of Fig. 14 correspond to the change of $-\text{Im}\,\omega$ with respect to l for the cases of $N = 1/2$ and $N = 1$, respectively. We note that the real parts of two cases have similar behaviors, so do the negative imaginary parts. In the left diagram $\text{Re}\,\omega$ depends on l linearly, and the slope is approximately 0.66 and 0.73 for the cases of $N = 1/2$ and $N = 1$, respectively. We deduce that the oscillating frequency of case $N = 1/2$ is smaller than that of case $N = 1$ for a fixed l, and that the difference of oscillating frequency

between the two cases becomes large when l increases. In the right diagram $-\text{Im}(\omega)$ has a peak at $l = 2$, where the peak is approximately 0.63 for the case of $N = 1/2$ and 0.56 for the case of $N = 1$; in particular, $-\text{Im}(\omega)$ goes to constant when $l \geq 5$, which equals 0.61 and 0.55 for the cases of $N = 1/2$ and $N = 1$, respectively. We deduce that the damping time (inversely proportional to $-\text{Im}(\omega)$) of the former case is smaller than that of the latter, and that there exists a minimum damping time at $l = 2$ for the two cases. We further know that our ARBH model is more stable in the case of $N = 1$ than in the case of $N = 1/2$ for a fixed l, where the minimum damping time at the peak corresponds to the state with the least stability, and that the stability decreases quickly when l takes values from one to two, and increases slowly when l takes values from two to five, and finally maintains unchanged when $l \geq 5$ for the two cases.

In Fig. 15, we draw the results of the QNMs depending on the characteristic parameter L, where $l = 3$ and $n = 0$ are
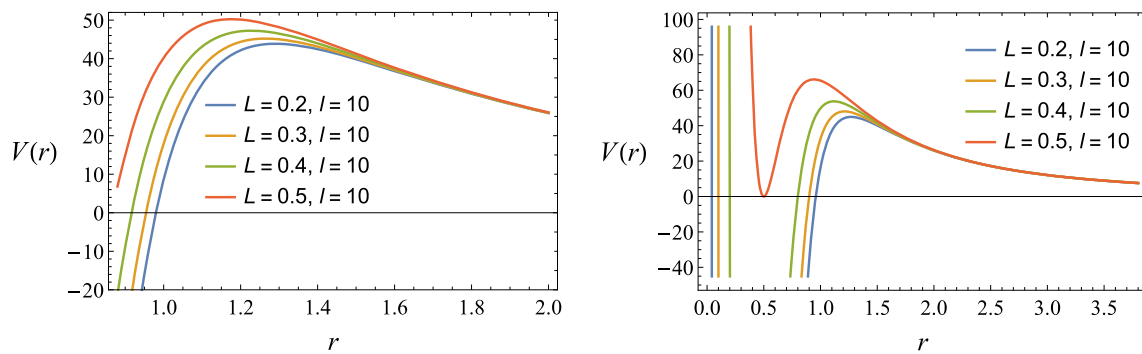
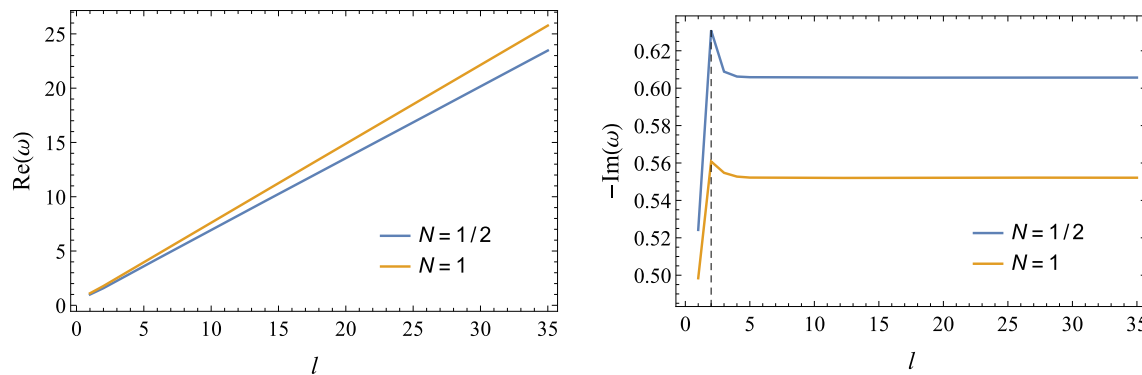**Fig. 13** $V(r)$ with respect to r for the cases of $N = 1/2$ (left) and $N = 1$ (right)

Fig. 14 QNMs with respect to l, where $L = 0.45$ and $n = 0$ are set. The left diagram represents the real parts of ω with respect to l for the cases of $N = 1/2$ and $N = 1$, respectively; the right diagram represents the negative imaginary parts of ω with respect to l for the cases of $N = 1/2$ and $N = 1$, respectively

set. For the two cases of $N = 1/2$ and $N = 1$, the real parts increase while the negative imaginary parts decrease when L increases. For a fixed L, the real part of case $N = 1/2$ is smaller than that of case $N = 1$, which shows that the oscillating frequency for the former is smaller than that for the latter after our ARBH model is perturbed; when L becomes large, the difference of oscillating frequency between the two cases becomes large. However, the negative imaginary part of case $N = 1/2$ is larger than that of case $N = 1$ for a fixed L, which shows that the damping time for the former is smaller than that for the latter; when L becomes large, the difference of damping time between the two cases also becomes large. In addition, our ARBH model is stable after it is perturbed because the imaginary part is negative, and it is more stable in the case of $N = 1$ than in the case of $N = 1/2$ for a fixed L, and on the other hand it is more stable for a larger L in the both cases.

We also calculate the QNMs of CRSBHs and compare them with those of the ARBH. In Fig. 16, we draw the results with respect to the multiple number l in the cases of $\bar{N} = 3/4$ and $\bar{N} = 1$, respectively. In the left diagram of Fig. 16, we find that the real parts of QNMs increase when l increases, which is similar to that of the ARBH. The right

diagram of Fig. 16 shows that the negative imaginary parts decrease monotonically when l increases. However, we note that the negative imaginary parts of the ARBH oscillate when l increases and reach the maximum at $l = 2$, see Fig. 14 for the details.

At last, we investigate the QNMs of CRSBHs with respect to $\bar{L}$ and compare them with those of the ARBH. We plot Fig. 17 for the two cases of $\bar{N} = 3/4$ and $\bar{N} = 1$, where the real parts decrease while the negative imaginary parts increase when $\bar{L}$ increases. For a fixed $\bar{L}$, the real part of case $\bar{N} = 3/4$ is larger than that of case $\bar{N} = 1$, which shows that the oscillating frequency for the former is larger than that for the latter after a CRSBH is perturbed; when $\bar{L}$ becomes large, the difference of oscillating frequency between the two cases also becomes large. On the other hand, the negative imaginary part of case $\bar{N} = 3/4$ is smaller than that of case $\bar{N} = 1$ for a fixed $\bar{L}$, which shows that the damping time for the former is larger than that for the latter; when $\bar{L}$ becomes large, the difference of damping time between the two cases also becomes large. Comparing Fig. 15 with Fig. 17, we find that the relative positions of the blue and orange curves are just opposite and the changes of them with respect to L and $\bar{L}$ are opposite, too.
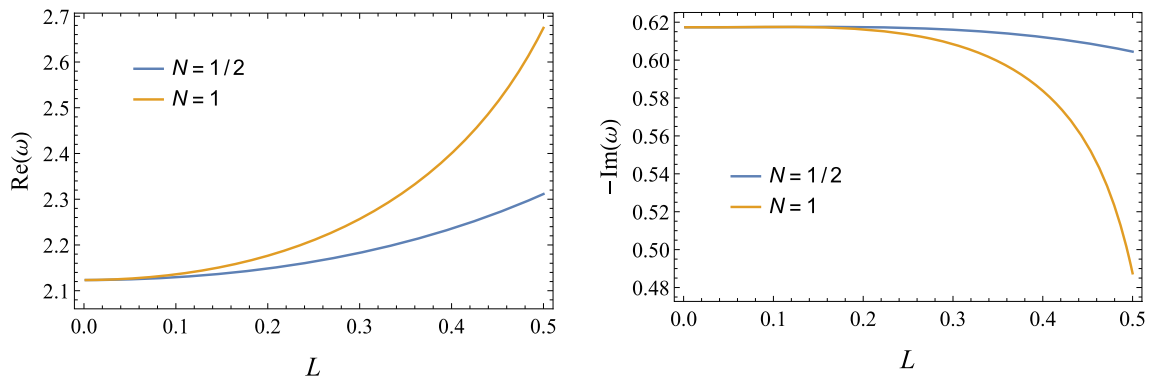
Fig. 15 QNMs with respect to L, where $l = 3$ and $n = 0$ are set. The left diagram represents the real parts of ω with respect to L for the cases of $N = 1/2$ and $N = 1$, respec- tively; the right diagram represents the negative imaginary parts of ω with respect to L for the cases of $N = 1/2$ and $N = 1$, respectively
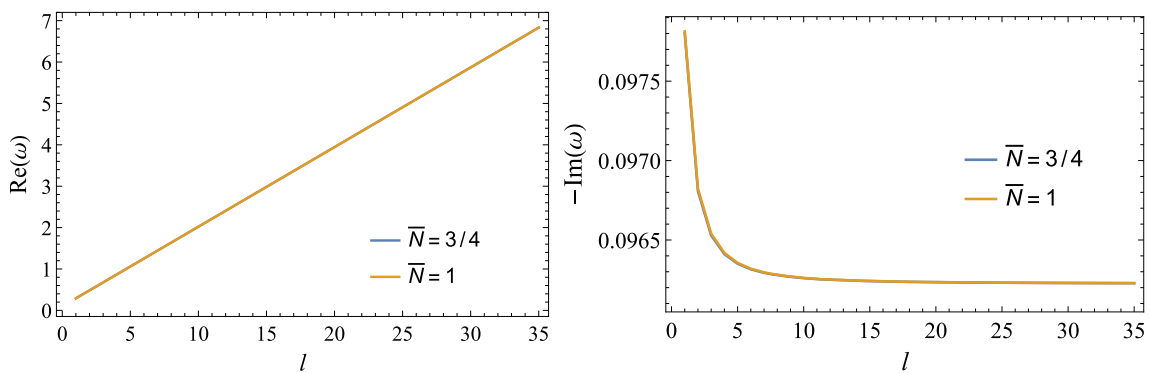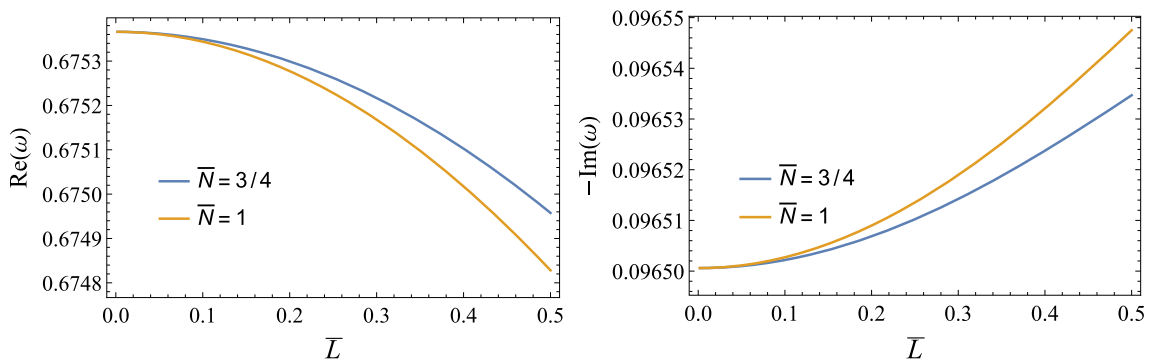

Fig. 16 QNMs of CRSBHs with respect to l, where $\bar{L} = 0.45$ and $n = 0$ are set. The left diagram represents the real parts of ω with respect to l for the cases of $\bar{N} = 3/4$ and $\bar{N} = 1$, respectively; the right diagram represents the negative imaginary parts of ω with respect to l for the cases of $\bar{N} = 3/4$ and $\bar{N} = 1$, respectively. Note that the curves of the two cases are almost overlapped

Fig. 17 QNMs of CRSBHs with respect to $\bar{L}$, where $l = 3$ and $n = 0$ are set. The left diagram represents the real parts of ω with respect to $\bar{L}$ for the cases of $\bar{N} = 3/4$ and $\bar{N} = 1$, respectively; the right diagram represents the negative imaginary parts of ω with respect to $\bar{L}$ for the cases of $\bar{N} = 3/4$ and $\bar{N} = 1$, respectively

7 Summary

In the present work, we construct a general ARBH model in the spherically symmetric fluid. Unlike the current ABH model [21] whose velocity of fluid diverges at $r = 0$, our model has a finite velocity but divergent density, where the density plays the role of the scale factor of a conformally related BH. The fluid flow is realized with the aid of a certain external field, which may offer a possibility to produce ARBHs in laboratory. Moreover, we give the valid domains

of various energy conditions. As we have shown in Fig. 9, the violated domains of the strong energy condition are located outside the horizon rather than inside the horizon, which may change our current knowledge on the relation between the regularity and strong energy condition. In addition, we compare our ARBH model with conformally related BHs in the aspect of energy conditions, and find the similarity and diversity between the two types of BHs.

In order to study ARBHs experimentally, it is necessary to analyze the QNMs of ARBHs. Using the WKB method, we calculate the QNMs of our ARBH model characterized by Eq. (22) in the cases of $N = 1/2$ and $N = 1$. The results show that the imaginary parts of QNMs are negative, which implies that our ARBH model is stable after it is perturbed. Moreover, the detail features of oscillating frequency and damping time are also given. In particular, we reveal the dependence of stability on the characteristic length of the scale factor (the density of fluid), L, i.e., our ARBH model is more stable for a larger L. When N is larger, the oscillation is faster. In summary, we have shown that the acoustic gravity is able to be employed as a means of studying the scalar perturbation of RBHs.

The simulation method we proposed is suitable for a large class of RBHs and provides a basis for further researches of the Hawking radiation and superradiance. Meanwhile, there is plenty of room for improvement in our method if we strictly follow certain physical principles, such as maintaining the energy conditions, which will be reported soon in our next work.

In addition, our further considerations also focus on the divergence of the classical action in the ARBH model we construct. This issue may lead to a vanishing partition function. Since the metric of our ARBH model has a conformal structure, we try to deal with the issue in the framework of conformal gravity, where the divergence will be improved when a scalar field is introduced. This will be reported elsewhere.

Data Availability Statement This manuscript has no associated data or the data will not be deposited. [Authors' comment: There are no experimental data attached to this paper. All figures are plotted from numerically generated data, which can be repeated by a computer algebra system, e.g. Mathematica.]

A Energy conditions of CRSBHs

In this appendix, we reanalyze the energy conditions of CRSBHs which have been considered in Ref. [35]. Because the sign of the energy density is wrong in Ref. [35], all the energy conditions related to it have to be reconsidered.

A.1 The difference between $T^\mu{}_\nu$ and $e^{(a)}_\mu T^{\mu\nu} e^{(b)}_\nu$

Let us start with the perfect fluid whose energy–momentum tensor takes the form,

$$T^{\mu\nu} = (\rho_0 + p)U^\mu U^\nu + pg^{\mu\nu}, \tag{66}$$

where $g_{\mu\nu}U^\mu U^\nu = -1$. In the rest frame, one can set $U^\mu = (1/\sqrt{-g_{00}}, 0, 0, 0)$, thus the diagonalized form can be written as

$$T^\mu{}_\nu = (\rho_0 + p)U^\mu U_\nu + p\delta^\mu_\nu, \tag{67}$$

namely,

$$T^0{}_0 = \frac{G^0{}_0}{8\pi} = -\rho_0, \qquad T^i{}_j = \frac{G^i{}_j}{8\pi} = p\delta^i_j. \tag{68}$$

Therefore, one has

$$T^\mu{}_\nu = \text{diag}\{-\rho_0, p, p, p\}, \tag{69}$$

where the 00 component of $T^\mu{}_\nu$ is negative energy density and the trace of $T^\mu{}_\nu$ equals

$$\text{Tr } T^\mu{}_\nu = -\rho_0 + 3p. \tag{70}$$

Alternatively, one can diagonalize $T^{\mu\nu}$ by using orthonormal tetrads. If the metric is diagonal, $g_{\mu\nu} = \text{diag}\{g_{tt}, g_{rr}, g_{\theta\theta}, g_{\phi\phi}\}$, the tetrads $e^{(a)}_\mu$ are of the following form,

$$e^{(a)}_\mu = \text{diag}\left\{\sqrt{-g_{tt}}, \sqrt{g_{rr}}, \sqrt{g_{\theta\theta}}, \sqrt{g_{\phi\phi}}\right\}. \tag{71}$$

Using Eq. (71), one can get

$$e^{(0)}_\mu T^{\mu\nu} e^{(0)}_\nu = \rho_0, \qquad e^{(i)}_\mu T^{\mu\nu} e^{(j)}_\nu = p\delta^i_j. \tag{72}$$

Therefore, an alternative diagonalized form is

$$e^{(a)}_\mu T^{\mu\nu} e^{(b)}_\nu = \text{diag}\{\rho_0, p, p, p\}, \tag{73}$$

and the corresponding trace is

$$\text{Tr } e^{(a)}_\mu T^{\mu\nu} e^{(b)}_\nu = \rho_0 + 3p. \tag{74}$$

A.2 The correct sign of the energy density of CRSBHs

For the CRSBHs, the metric is

$$g_{\mu\nu} = S(r) \, \text{diag}\{-f, f^{-1}, r^2, r^2 \sin^2\theta\}, \tag{75}$$

where

$$S(r) = \left(1 + \frac{\bar{L}^2}{r^2}\right)^{2\bar{N}}, \qquad f(r) = 1 - \frac{2M}{r}. \tag{76}$$

The 00 component of $T^\mu{}_\nu$ can be computed,

$$T^0{}_0 = -\rho_0 = -e^{(0)}_\mu T^{\mu\nu} e^{(0)}_\nu = \frac{4\bar{L}^2 \bar{N} r^{4\bar{N}-3}}{8\pi \left(\bar{L}^2 + r^2\right)^{2(\bar{N}+1)}}$$
$$\times \left[\bar{L}^2 \left(-2M\bar{N} + M + \bar{N}r - r\right) + r^2(r - 3M)\right], \tag{77}$$

namely, the energy density is

$$\rho_0 = -\frac{4\bar{L}^2 \bar{N} r^{4\bar{N}-3}}{8\pi \left(\bar{L}^2 + r^2\right)^{2(\bar{N}+1)}}$$
$$\times \left[\bar{L}^2(-2M\bar{N} + M + \bar{N}r - r) + r^2(r - 3M)\right], \tag{78}$$

which is different from Eq. (A.1) of Ref. [35] up to a minus sign. Thus, all the inequalities will be different, e.g.,

$$\rho_0 + \sum_{i=1}^{3} p_i = -\frac{4\bar{L}^2 \bar{N} r^{4\bar{N}-3}}{8\pi \left(\bar{L}^2 + r^2\right)^{2(\bar{N}+1)}}$$
$$\times \left[\bar{L}^2(M(8\bar{N}+2) - (4\bar{N}-1)r) - (r - 6M)r^2\right] \tag{79}$$

is different from Eq. (33) of Ref. [35].

B Energy conditions of the toy model $f(r) = 1 - r^n$

In order to analyze the SEC and DEC outside the event horizon, we analyze the model with the metric,

$$g_{\mu\nu} = \text{diag}\left\{-(1 - r^n), (1 - r^n)^{-1}, r^2, r^2 \sin^2\theta\right\}, \tag{80}$$

where $n \in \mathbb{R}$. The SEC is then represented via ρ_0 and P_i $(i = 1, 2, 3)$,

$$\rho_0 + P_1 = 0, \tag{81}$$

$$\rho_0 + P_2 = \rho_0 + P_3 = -\frac{(n-2)(n+1)}{16\pi} r^{n-2}, \tag{82}$$

$$\rho_0 + \sum_{i=1}^{3} P_i = -\frac{n(n+1)}{8\pi} r^{n-2}. \tag{83}$$

From Eqs. (81)–(83), we note that n must satisfy $-1 \le n \le 0$ in order to ensure that the SEC is satisfied. For the DEC, one

has the following form,

$$\rho_0 - |P_1| = \frac{(n+1 - |n+1|)}{8\pi} r^{n-2}, \tag{84}$$

$$\rho_0 - |P_2| = \frac{(2n+2 - |n||n+1|)}{16\pi} r^{n-2}, \tag{85}$$

which leads to $-1 \le n \le 2$ if the DEC is satisfied. For our ARBH model, the metric function is asymptotic to $1 - 1/r^4$ at infinity, i.e., $n = -4$, which means that both SEC and DEC are violated outside the event horizon.

From the point of view of Raychaudhuri's equation [47], when the expansion, rotation, and shear can be neglected, one obtains

$$\frac{\mathrm{d}\xi}{\mathrm{d}\tau} = -4\pi \left(\rho_0 + \sum_{i=1}^{3} P_i\right), \tag{86}$$

where ξ denotes expansion of geodesics and τ affine parameter. The violation of Eq. (83) implies $\mathrm{d}\xi/\mathrm{d}\tau > 0$, i.e., the gravity is repulsive outside the horizon for $n = -4$.

References

1. S.W. Hawking, Black hole explosions? Nature **248**, 30 (1974)
2. W.G. Unruh, Experimental black-hole evaporation? Phys. Rev. Lett. **46**, 1351 (1981)
3. M. Visser, Acoustic black holes: Horizons, ergospheres and Hawking radiation. Class. Quantum Gravity **15**, 1767 (1998). arXiv:gr-qc/9712010
4. L.J. Garay, J.R. Anglin, J.I. Cirac, P. Zoller, Sonic analog of gravitational black holes in Bose-Einstein condensates. Phys. Rev. Lett. **85**, 4643 (2000). arXiv:gr-qc/0002015
5. S. Weinfurtner, E.W. Tedford, M.C.J. Penrice, W.G. Unruh, G.A. Lawrence, Measurement of stimulated Hawking emission in an analogue system. Phys. Rev. Lett. **106**, 021302 (2011). arXiv:1008.1911 [gr-qc]
6. J. Drori, Y. Rosenberg, D. Bermudez, Y. Silberberg, U. Leonhardt, Observation of stimulated Hawking radiation in an optical analogue. Phys. Rev. Lett. **122**, 010404 (2019). arXiv:1808.09244 [gr-qc]
7. R.-Q. Yang, H. Liu, S. Zhu, L. Luo, R.-G. Cai, Simulating quantum field theory in curved spacetime with quantum many-body systems. Phys. Rev. Research **2**, 023107 (2020). arXiv:1906.01927 [gr-qc]
8. C. Barceló, S. Liberati, M. Visser, Analogue gravity. Living Rev. Relativ. **14**, 3 (2011). arXiv:gr-qc/0505065
9. J. Steinhauer, Observation of quantum Hawking radiation and its entanglement in an analogue black hole. Nature Phys. **12**, 959 (2016). arXiv:1510.00621 [gr-qc]
10. L.P. Euvé, F. Michel, R. Parentani, T.G. Philbin, G. Rousseaux, Observation of noise correlated by the Hawking effect in a water tank. Phys. Rev. Lett. **117**, 121301 (2016). arXiv:1511.08145v4 [physics.flu-dyn]
11. L.-P. Euvé, S. Robertson, N. James, A. Fabbri, G. Rousseaux, Scattering of co-current surface waves on an analogue black hole. Phys. Rev. Lett. **124**, 141101 (2020). arXiv:1806.05539v3 [gr-qc]
12. J.R.M. de Nova, K. Golubkov, V.I. Kolobov, J. Steinhauer, Observation of thermal Hawking radiation and its temperature in an analogue black hole. Nature **569**, 688 (2019). arXiv:1809.00913 [gr-qc]

13. V.I. Kolobov, K. Golubkov, J.R.M. de Nova, J. Steinhauer, Observation of stationary spontaneous Hawking radiation and the time evolution of an analogue black hole. Nature Phys. **17**, 362 (2021). arXiv:1910.09363 [gr-qc]

14. X.-H. Ge, S.-F. Wu, Y. Wang, G.-H. Yang, Y.-G. Shen, Acoustic black holes from supercurrent tunneling. Int. J. Mod. Phys. D **21**, 1250038 (2012). arXiv:1010.4961 [gr-qc]

15. T. Torres, S. Patrick, A. Coutant, M. Richartz, E.W. Tedford, S. Weinfurtner, Observation of superradiance in a vortex flow. Nature Phys. **13**, 833 (2017). arXiv:1612.06180 [gr-qc]

16. M.C. Braidotti, R. Prizia, C. Maitland et al., Measurement of Penrose Superradiance in a Photon Superfluid. Phys. Rev. Lett. **128**, 013901 (2022). arXiv:2109.02307 [physics.optics]

17. T. Torres, S. Patrick, M. Richartz, S. Weinfurtner, Quasinormal mode oscillations in an analogue black hole experiment. Phys. Rev. Lett. **125**, 011301 (2020). arXiv:1811.07858 [gr-qc]

18. Q.-B. Wang, X.-H. Ge, Geometry outside of acoustic black holes in (2+1)-dimensional spacetime. Phys. Rev. D **102**, 104009 (2020). arXiv:1912.05285 [hep-th]

19. X.-H. Ge, M. Nakahara, S.-J. Sin, Y. Tian, S.-F. Wu, Acoustic black holes in curved spacetime and the emergence of analogue Minkowski spacetime. Phys. Rev. D **99**, 104047 (2019). arXiv:1902.11126 [hep-th]

20. C.C. de Oliveira, R.A. Mosna, J.P.M. Pitelli, M. Richartz, Analogue models for Schwarzschild and Reissner-Nordström spacetimes. Phys. Rev. D **104**, 024036 (2021). arXiv:2106.03960 [gr-qc]

21. E. Berti, V. Cardoso, J.P. Lemos, Quasinormal modes and classical wave propagation in analogue black holes. Phys. Rev. D **70**, 124006 (2004). arXiv:gr-qc/0408099

22. C.-Y. Chen, P. Chen, Gravitational perturbations of nonsingular black holes in conformal gravity. Phys. Rev. D **99**, 104003 (2019). arXiv:1902.01678 [gr-qc]

23. V.P. Frolov, Notes on nonsingular models of black holes. Phys. Rev. D **94**, 104056 (2016). arXiv:1609.01758 [gr-qc]

24. S. Ansoldi, Spherical black holes with regular center: A review of existing models including a recent realization with Gaussian sources. arXiv:0802.0330 [gr-qc]

25. J. M. Bardeen, Non-singular general-relativistic gravitational collapse, in Proc. Int. Conf. GR5, Tbilisi, vol. 174, (1968)

26. E. Ayón-Beato, A. García, The Bardeen model as a nonlinear magnetic monopole. Phys. Lett. B **493**, 149 (2000). arXiv:gr-qc/0009077

27. K.A. Bronnikov, V.N. Melnikov, G.N. Shikin, K.P. Staniukowicz, Scalar, electromagnetic, and gravitational fields interaction: Particlelike solutions. Ann. Phys. **118**, 84 (1979)

28. E. Ayón-Beato, A. García, Regular black hole in general relativity coupled to nonlinear electrodynamics. Phys. Rev. Lett. **80**, 5056 (1998). arXiv:gr-qc/9911046

29. Z.-Y. Fan, X. Wang, Construction of regular black holes in general relativity. Phys. Rev. D **94**, 124027 (2016). arXiv:1610.02636 [gr-qc]

30. S.A. Hayward, Formation and evaporation of regular black holes. Phys. Rev. Lett. **96**, 031103 (2006). arXiv:gr-qc/0506126

31. I. Dymnikova, Vacuum nonsingular black hole. Gen. Rel. Grav. **24**, 235 (1992)

32. V.P. Frolov, A. Zelnikov, Quantum radiation from an evaporating nonsingular black hole. Phys. Rev. D **95**, 124028 (2017). arXiv:1704.03043 [hep-th]

33. R. Konoplya, A. Zhidenko, Quasinormal modes of black holes: From astrophysics to string theory. Rev. Mod. Phys. **83**, 793 (2011). arXiv:1102.4014 [gr-qc]

34. C. Bambi, L. Modesto, L. Rachwał, Spacetime completeness of non-singular black holes in conformal gravity. JCAP **05**, 003 (2017). arXiv:1611.00865 [gr-qc]

35. B. Toshmatov, C. Bambi, B. Ahmedov, A. Abdujabbarov, Z. Stuchlík, Energy conditions of non-singular black hole spacetimes in conformal gravity. Eur. Phys. J. C **77**, 542 (2017). arXiv:1702.06855 [gr-qc]

36. Y. Li, Y.-G. Miao, Distinct thermodynamic and dynamic effects produced by scale factors in conformally related Einstein-power-Yang-Mills black holes. Phys. Rev. D **104**, 024002 (2021). arXiv:2102.12292 [gr-qc]

37. S.W. Hawking, G.E.R. Ellis, *The large scale structure of spacetime* (Cambridge University Press, Cambridge, 1973)

38. E. Poisson, *A relativist's toolkit: The mathematics of black-hole mechanics* (Cambridge University Press, Cambridge, 2004)

39. W. Unruh, Separability of the neutrino equations in a Kerr background. Phys. Rev. Lett. **31**, 1265 (1973)

40. Y. Guo, Y.-G. Miao, Quasinormal mode and stability of optical black holes in moving dielectrics. Phys. Rev. D **101**, 024048 (2020). arXiv:1911.04479 [gr-qc]

41. B.F. Schutz, C.M. Will, Black hole normal modes: A semianalytic approach. Astrophys. J. **291**, L33 (1985)

42. S. Iyer, Black-hole normal modes: A WKB approach. II. Schwarzschild black holes. Phys. Rev. **D 35**, 3632 (1987)

43. S. Iyer, C.M. Will, Black-hole normal modes: A WKB approach. I. Foundations and application of a higher-order WKB analysis of potential-barrier scattering. Phys. Rev. **D 35**, 3621 (1987)

44. E. Berti, V. Cardoso, A.O. Starinets, Quasinormal modes of black holes and black branes. Class. Quantum Gravity **26**, 163001 (2009). arXiv:0905.2975 [gr-qc]

45. R. Konoplya, Quasinormal behavior of the D-dimensional Schwarzschild black hole and the higher order WKB approach. Phys. Rev. D **68**, 024018 (2003). arXiv:gr-qc/0303052

46. L. Modesto, and L. Rachwal, Finite conformal quantum gravity and nonsingular spacetimes. arXiv:1605.04173 [hep-th]

47. S.M. Carroll, *Spacetime and geometry: An introduction to general relativity* (Addison-Wesley, New York, 2004)

48. O.B. Zaslavskii, Regular black holes and energy conditions. Phys. Lett. B **688**, 278 (2010). arXiv:1004.2362 [gr-qc]

49. G.W. Gibbons, S.W. Hawking, Action integrals and partition functions in quantum gravity. Phys. Rev. D **15**, 2752 (1977)

50. M.P. Dabrowski, J. Gareckil, D.B. Blaschke, Conformal transformations and the conformal invariance in gravitation. Ann. Phys. (Berlin) **18**, 13 (2009)